

Article

# Study of the Composition and Properties of Bivalve Mollusk Shells as Promising Bio-Indifferent Materials for Photocatalytic Applications (Example of Practical Use)

Aleksey V. Zaitsev <sup>1,\*</sup>  and Ivan A. Astapov <sup>2</sup> <sup>1</sup> Institute of Water and Ecology Problems FEB RAS, Khabarovsk 680000, Russia<sup>2</sup> Institute of Tectonics and Geophysics FEB RAS, Khabarovsk 680000, Russia; astapov-itig@mail.ru

\* Correspondence: alex-im@mail.ru

**Abstract:** This paper studies the composition and properties of shells of bivalve mollusks (*Crenomytilus grayanus*, *Callista brevisiphonata*, and *Mizuhopecten yessoensis*) from coastal discharges with a view to the possibility of their use in photocatalytic water treatment systems. The clam shells are considered in terms of application in the form of a powder material as a precursor for creating photocatalysts, and also as a carrier of photocatalytic coatings. It was shown that the main phase composing the shell material was calcium carbonate in two crystallographic modifications—calcite and aragonite. The presence of inorganic impurities in all studied clam shells did not exceed one mass percent. The main share was made up of elements included in the composition of calcium carbonate, which confirmed the high bio-indifference of the materials under study. Depending on the physiological and environmental features of the structure of clam shells, different contents of the organic component in their composition were observed. The granulometric characteristics of crushed clam shells (average diameter, specific surface area, and distribution modality) were studied. It was shown that the maximum values of bending strength of 5 MPa and compressive strength of 2 MPa are characterized by *Mizuhopecten yessoensis* shells with the lowest porosity of 2.91%. The features of sorption and photosorption processes of both whole and crushed shells in relation to four organic dyes at different temperatures and degrees of illumination were studied. Based on crushed shells of *Mizuhopecten Yessoensis* and titanium dioxide, functional materials ( $\text{Ca}_x\text{Ti}_y\text{O}_z$ ) were obtained, and their morphology and photocatalytic properties were studied. An example of the practical use of clam shells as a carrier of a photocatalytic coating is given.

**Keywords:** clam shell; photocatalytic water treatment; bio-indifferent carriers; organic dyes; functional properties



**Citation:** Zaitsev, A.V.; Astapov, I.A. Study of the Composition and Properties of Bivalve Mollusk Shells as Promising Bio-Indifferent Materials for Photocatalytic Applications (Example of Practical Use). *Catalysts* **2024**, *14*, 16. <https://doi.org/10.3390/catal14010016>

Academic Editor: Detlef W. Bahnemann

Received: 9 November 2023

Revised: 28 November 2023

Accepted: 22 December 2023

Published: 24 December 2023



**Copyright:** © 2023 by the authors. Licensee MDPI, Basel, Switzerland. This article is an open access article distributed under the terms and conditions of the Creative Commons Attribution (CC BY) license (<https://creativecommons.org/licenses/by/4.0/>).

## 1. Introduction

The annual accumulation of pollutants of organic and inorganic nature in the air, water and soil is continuously raising environmental risks for the habitat of animals and men [1]. The balance between rational nature management and commercial profit from using natural resources in various production chains in most cases turns out to be disrupted. One of the most used natural resources applied in different stages of industrial production is water. The water resources of our planet in combination with water ecosystems are permanently being involved in various technology processes of national-economic human activities. There is much concern about the pure water deficiency in many countries of the world [2]. In connection with that, the modern development of industrial production sets for the research teams new tasks for creating highly effective water treatment technologies with low cost/high value and high environmental safety. In the past several decades, much research support has been given to a promising new direction in the treatment of polluted water effluents with the use of solar photocatalysts [3,4]. The method of photocatalytic

purification of water from organic pollutants per se is the ability of photocatalysts to effectively transform the energy of solar radiation energy into the energy of chemical interaction. As a result of such a redistribution of energy, the photocatalyst is able to generate, in an aqueous medium, highly reactive particles (hydroxide radical, atomic oxygen, and superoxide anion), which can effectively destroy organic molecules of pollutants for safe water and carbon dioxide [5]. At the present time, the effectiveness of a large number of photocatalytic materials capable of destroying various organic pollutants when exposed to solar radiation has been shown [6–9]. However, the methods of receiving most of the described photocatalysts are multistage and expensive due to the use of high-cost starting components. At the same time, the desire to improve the functional efficiency of the materials obtained makes the researcher use, in the photocatalyst synthesis, substances based on heavy and toxic elements with high eco-risks to the habitat of animals and humans. Thus, for instance, well known are the works for creating high-efficiency photocatalysts to purify water from organic pollutants with use of compounds of thallium [10–13], mercury [14–16], lead [17–19], cadmium [20,21], uranium [22], and thorium [23]. The most promising solution to this problem is the application of the “green” synthesis method when receiving the compounds under study. This method per se involves applying, as initial components, the substances created by nature (extracts from various organisms, minerals, mineralized remain and etc.), having a low cost/high value and high safety for the environment [24–27]. The search for initial components of photocatalysts based on the compounds of plant or animal origin is currently an important way to improve the functional properties of photocatalytic materials in terms of environmental safety. Thus, for example, available are the studies using animal eggshells as initial material in the synthesis of photocatalysts based on calcium titanate [28]. Calcium titanate, in its turn, is a bio-indifferent material (enters the composition of prosthetic materials) possessing photocatalytic activity and having other prospective areas of application [29]. Calcium carbonate is also the main component of the exoskeleton of marine and freshwater invertebrates [30], and there are prospects for using this material both as a bio-indifferent carrier of photocatalytic coatings and as an initial material at the photocatalyst synthesis [31]. Due to the low cost/high value, the calcium carbonate-based natural materials have already been actively applied in other areas of national economy as preparations for food products [32] or additives for animal feed [33]. At the same time, the calcium compounds are initial components for the synthesis of bismuth photocatalysts, such as solid solutions of calcium bismuthates of various stoichiometries [34–36], also offering prospects for using the exoskeleton of invertebrates in manufacturing eco-friendly bismuth photocatalysts. On the other hand, a known problem holding back the wide use of photocatalysts industrially is covering an industrial carrier with a functional photocatalytic coating made of powder materials. The selection of the carrier for the photocatalytic coating is a complicated complex task, since it requires considering a multitude of factors [37]. To ensure the coating’s durability, the photoactive layer must have sufficient adhesion to the carrier’s surface. At the same time, the excessive interaction of the photocatalyst material with the carrier is not desirable, as it leads to changes in the chemical composition of the coating and the partial loss of its activity. To address such problems, special middle layers are created that separate the catalyst and its carrier but preserve its high adhesion to both. However, the creation of middle layers of various composition complicates the technology of receiving photoactive material and increases its end-value. An alternative way of creating a photoactive layer is by matching carrier and precursor substances, in which, as a result of chemical interaction, the photocatalytically active coating is formed in one stage [38]. The most relative direction solving the problem of covering a carrier with a photocatalyst coating is the use of chemically complementary compounds of the carrier’s material and the material of the initial components of photocatalysts [39]. The range of the reference literature data on the problems of using the elements of exoskeletons of marine and freshwater invertebrates as a bio-indifferent carrier of photocatalytic coatings is nondescript and yields little information, offering perspectives of scientific studies in this direction and justifying the novelty of the

current research. The applied methods for covering industrial carriers with photocatalytic materials [37,38,40] in their majority result in the thermal destruction of the carrier (coating) and the loss of its mechanical properties during further use in the conditions of industrial water-treatment facilities. Also, the carrier's material must not only be impact-resistant but also hydrolytically stable when used in solar water treatment plants with various structural peculiarities [41]. It is commonly known that the photocatalytic process includes three parallel stages running with different speeds [42]: 1—self-decomposition of an organic pollutant under the impact of quanta of photo-stimulating radiation; 2—sorption, photosorption processes on the photocatalyst's and carrier's surfaces; 3—photocatalytic decomposition of an organic pollutant under the impact of hydroxyl and oxygen radicals in the vicinity of the photocatalyst surface, and also decomposition under the exposure to photo-holes on the photocatalyst surface. The calcium carbonate-based materials received from clam shells are good sorbents both of organic molecules [43] and inorganic ions [44,45]. The studies of the sorption activity of the calcium carbonate-based materials in respect to widespread organic pollutants—methylene blue (MB) [46], methyl orange (MO) [47], rhodamine (R6G) [48], and malachite green (MG) [49]—used in simulated experiments are also important at the current stage of the development of the given method of water treatment. The described complex of problems of the photocatalytic water treatment method determines the objective and novelty of the current study. The main goal of the work is to consider the prospects for using the mineral skeleton of marine invertebrates as a starting material for photocatalytic applications by studying its composition and properties, as well as obtaining photocatalytic material based on it. The novelty of this research lies in the fact that, for the first time, a knowledge-intensive justification will be given for the use of bivalve mollusk shells as bio-indifferent: (1) precursors for the synthesis of photocatalysts and (2) carriers for photocatalytic coatings that are stable in an aqueous environment.

## 2. Results and Discussions

### 2.1. Options for Photocatalytic Applications

Functional properties are essential when implementing new materials in existing industrial systems. According to the scheme in Figure 1, photocatalytic materials can be divided into two big groups: (1) powder materials that are either precursors at the photocatalyst synthesis [28,50], or materials entering the composition of photocatalytic heterostructure-based compositions [35,51,52]; (2) solid materials that are either able to play a role of the photoactive coating carrier or show photocatalytic activity themselves [37,38]. The given classification determines the main area of application of the described materials. Powder materials are used in the processes of photocatalyst synthesis and their simulated experiments when solid materials are directly used in solar water-treatment plants. For each of the described areas, there is a set of essential functional properties of a material that can be studied through the use of instrumental analysis method (Figure 1). The most important functional properties of the powder materials (grinded clam shells) under consideration in this paper can be referred to as granulometric parameters ( $M_{od}$ ,  $D$ ,  $S_s$ ), which directly influence the following: rate of the processes of chemical synthesis or photocatalysis, rate of sorption/desorption processes, and processes of molding and pressing in production of volume materials. The presence of organic and inorganic impurities and the degree of purity of the purpose phase of a powder material are essential properties influencing the processes of chemical synthesis. The most important functional properties of the volume materials (clam shells) under consideration in the paper can be referred to as (Figure 1) strength properties (brittleness and grindability), hydrophobic/hydrophilic behavior (wettability), and curvature and morphology of a material surface turned to the sun. When using volume materials in the flowthrough water treatment plants of an enclosed type [53], where polluted water ends under pressure, the material strength is of great importance. The strength properties of the materials under consideration were evaluated via methods for calculating the ultimate strength of a material at  $\sigma_f$  and  $\sigma_c$ . On the other hand, for the open-type water treatment plant [41] (water sedimentation

tanks), due to their structural peculiarities related to the impossibility to turn the massive structure perpendicularly to the sun radiation during daylight, an important property of a carrier becomes the surface curvature and morphology. The choice of a side for applying photocatalytic coating to a carrier is also explained by the surface structure and morphology. The hydrophobic/hydrophilic behavior of a volume photocatalytic material or carrier of photocatalytic coating in the conditions of use in water treatment plants of both types has a substantial effect on the rate of physicochemical processes on their surface. It is known that photocatalytic processes are induced by solar radiation, and the bigger the water layer thickness in a water treatment facility, the lower the rate of photo-treatment. Such a problem can be solved either through designing facilities with a water layer thickness below 0.5 m or creating photoactive volume materials floating in the near-surface layer. A significant characteristic for creating floating materials is their initial  $\rho$ . The most important functional property both for powder and volume materials is bio-indifference. Water-treating materials of experimental powder photocatalyst must not pollute cleaned water with toxic elements entering their composition.

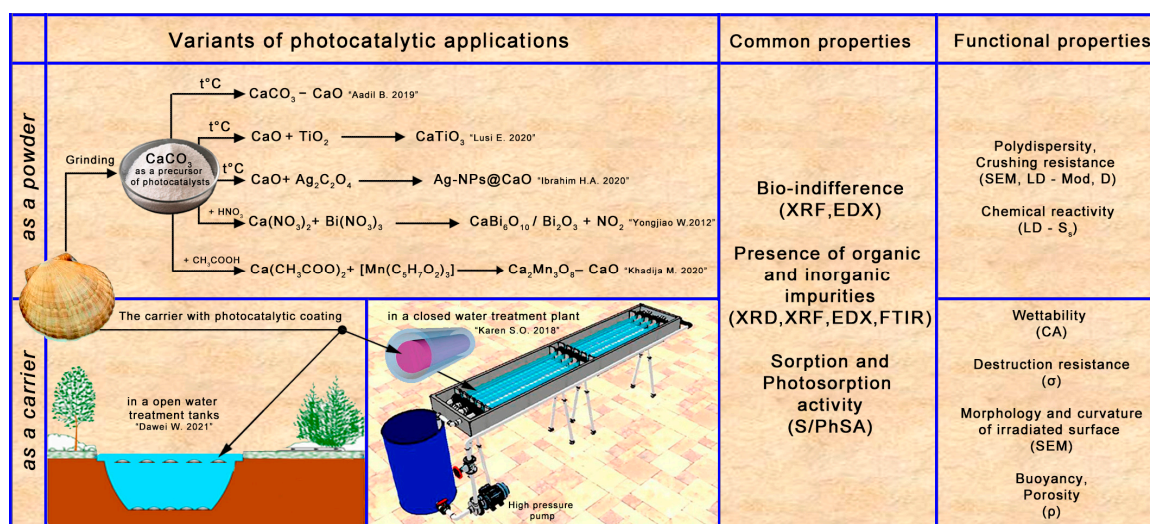


**Figure 1.** Scheme of common and functional properties of photocatalytic materials and methods of their measurement. Examples of photocatalytic systems based on calcium carbonate [28,35,50–52] and possible applications of photocatalytic coating carriers [41,53].

## 2.2. Characteristics Biological Items

The place of sampling was a rocky shore of the Sea of Japan in the section of the Peter the Great Gulf (Figure 2a). From the specified site, fragments of the mineral skeleton of dead invertebrates were collected and classified by their belonging to phyla, classes, and species according to the atlases and guides for the identification of animals inhabiting the specified territory [54,55]. Then, to determine the dominant species of invertebrates in coastal discharge, a distribution system was developed based on the gross ratio of mineral skeleton fragments depending on the species and class of the found animals (Figure 2b). Based on the obtained distribution, the animal class most frequently found in the sample from coastal discharge was the bivalve mollusk, and also about 2.4% of total weight fell within the classes *Gastropoda* and *Thecostraca*. The fragments of the mineral skeletons of bivalve mollusks equaled 68.6% of the total weight of all the fragments found in the sample of coastal discharges. The further development of distribution within the class of bivalve mollusks showed that the largest number of the mineral skeleton fragments belonged to three species of mollusks (Supplementary Figure S2): *Crenomytilus grayanus* (42%), *Callista brevisiphonata* (29%), and *Mizuhopecten yessoensis* (16%). In the coastal discharges under consideration, all the fragments of *Mizuhopecten yessoensis* belonged to lower camber shell. Furthermore, this paper considers only a lower shell of this mollusk.

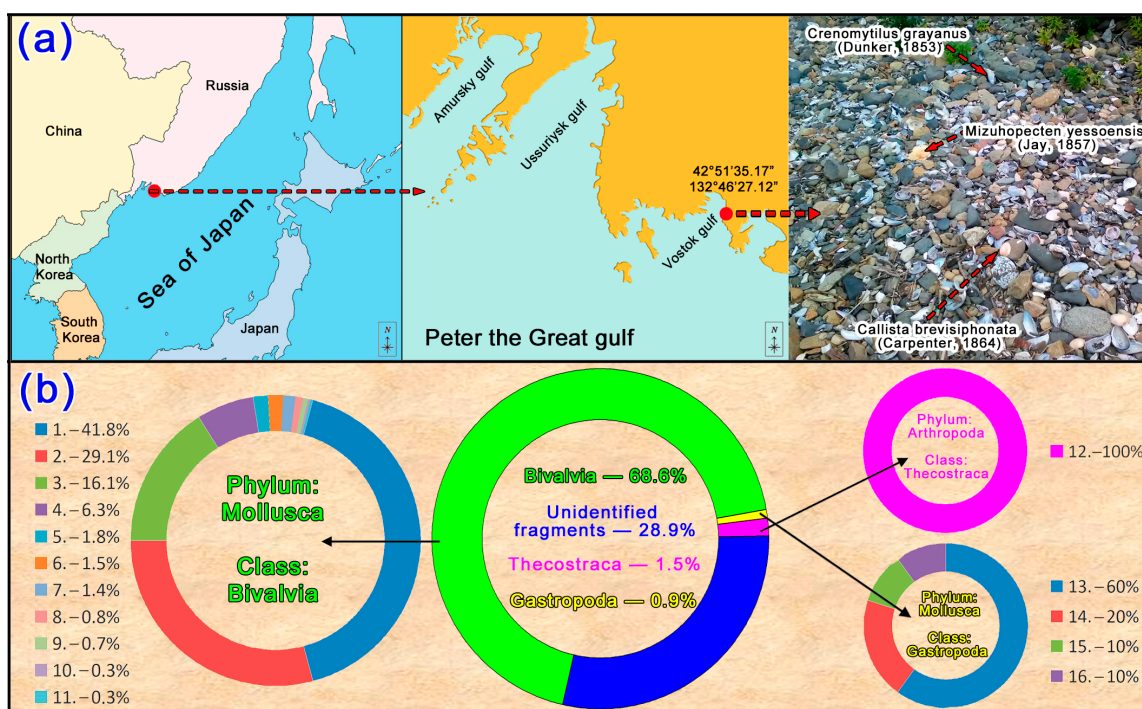


**Figure 2.** (a) The location of sampling of the mineral skeleton of invertebrates (example of coastal discharges). (b) Percentage mass distribution by classes (*Bivalvia*, *Gastropoda*, and *Thecostraca*) within two phyla (*Mollusca*, *Arthropoda*), as well as species of marine invertebrates in a sample from coastal discharges: (1) *Crenomytilus grayanus* (Dunker, 1853); (2) *Callista brevisiphonata* (Carpenter, 1864); (3) *Mizuhopecten yessoensis* (Jay, 1857); (4) *Saxidomus purpurata* (Sowerby II, 1852); (5) *Maetra quadrangularis* (Deshayes, 1854); (6) *Crassostrea gigas* (Thunberg, 1793); (7) *Glycymeris yessoensis* (Sowerby III, 1889); (8) *Maetra chinensis* (Philippi, 1846); (9) *Chlamys swiftii* (Bernardi, 1858); (10) *Spisula sachalinensis* (Schrenck, 1861); (11) *Protothaca jedoensis* (Lischke, 1874); (12) *Balanus hesperius* (Pilsbry, 1916); (13) *Nucella heyseana* (Dunker, 1882); (14) *Neptunea cuspidis* (Fraussen and Terry, 2007); (15) *Cryptonatica janthostoma* (Deshayes, 1839); (16) *Umbonium costatum* (Kiener, 1839).

#### *Crenomytilus grayanus*

Pacific Ocean, Asiatic, low boreal, sublittoral species. Inhabits various subsoils and depths from 1 to 60 m. Forms aggregations up to 500 specimen/m<sup>2</sup>. The shell is big, thick-walled, cambered. Has economic importance according to the shell's length, starting from 100 mm.

#### *Callista brevisiphonata*

Pacific Ocean, Asiatic, low boreal, sublittoral species. Inhabits gravel subsoil, less often sand at the depth of 4–60 m. Forms aggregations up to 17 specimen/m<sup>2</sup>. The shell is strong, oval, cambered, densely covered with shorter concentric ribs. Has economic importance according to the shell's length, starting from 70 mm.

#### *Mizuhopecten yessoensis*

Pacific Ocean, Asiatic, low boreal, sublittoral–eulittoral species. Inhabits silty sand, silty soil, and clean sand at a depth from 1 to 80 m. Forms aggregations of 7–30 specimen/m<sup>2</sup>. The shell has unequal valves. The lower valve is cambered, and the upper one is straight. The upper valve diameter is less than the lower. Both valves have 21–23 radial ribs each. Has economic importance according to the shell's length, starting from 100 mm.

### 2.3. Study of Composition and Properties

#### 2.3.1. Phase and Elemental Composition

The phase and elemental composition of the clam shells under study depend both on the biological peculiarities of the organism vitality and its habitat. Figure 3 shows

the data of the phase and elemental composition of powders of clam shells compared with industrial calcium carbonate, which is the main component of the mineral skeleton of the marine invertebrates under study. According to the method sensitivity, the XRD analysis of the grinded shell samples showed the presence of only calcium carbonate in two different crystallographic modifications—calcite (ICDD No. 47-1743) and aragonite (ICDD No. 41-1475). The ratio of calcite to aragonite depends on ecological, evolutionary, and age peculiarities of clams [56]. The phase composition (Figure 3a) of the shells of the clams under study was characterized by the prevalence of calcite in the composition of the *Mizuhopecten yessoensis* shells, prevalence of aragonite in the composition of the *Callista brevisiphonata* shells, and mixture of calcite and aragonite in the composition of the *Crenomytilus grayanus* shells. The semiquantitative analysis of the mass content of calcite showed the concentrations in the clam shells as follows: *Crenomytilus grayanus*—37%; *Callista brevisiphonata*—2%; and *Mizuhopecten yessoensis*—86%. The phase composition of the powder materials has a substantial effect on the rate and efficiency of the chemical synthesis processes in which the powders under study can be used as a precursor. According to the thermogravimetry data [57], calcite is the most stable phase of calcium carbonate and gets decomposed into carbon dioxide and calcium oxide at temperatures around 800–900 °C. Aragonite, in its turn, is a metastable phase of calcium carbonate and passes into calcite at temperatures around 450 °C [58]. However, according to the studies of the temperature stability of corals [59], the aragonite phase transformation temperature is able to decrease with respect to conventional values. At the same time, the decomposition temperature of calcium carbonate received from clam shells [60] is also able to decrease with respect to the decomposition temperature of the industrial calcium carbonate. Due to the described temperature peculiarities of the phases entering the composition of the mineral skeleton of marine invertebrates, the choice of shells as functional materials for photocatalytic application must be based on an obligatory study of the calcite-to-aragonite ratio.

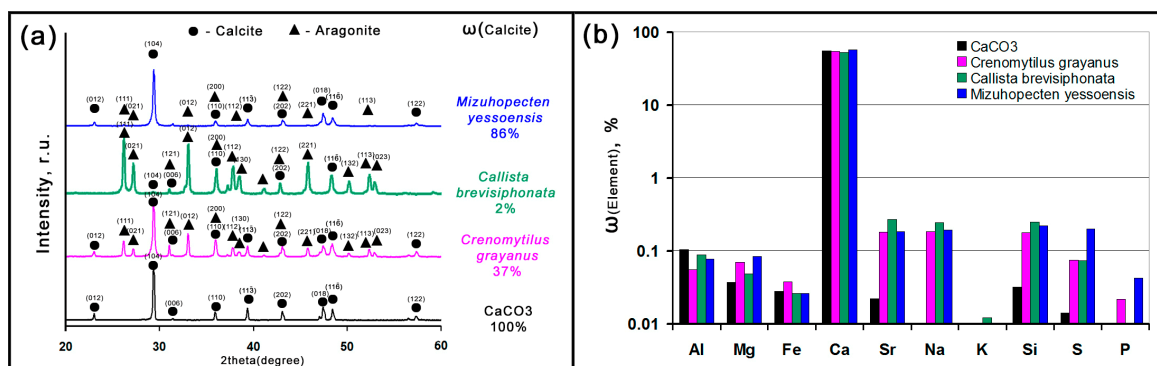


Figure 3. Phase (a) and elemental (b) composition of the studied invertebrate shells.

The presence of impurity atoms in the composition of precursor substances may have a significant effect both on the process of photocatalyst chemical synthesis and its photocatalytic activity [61]. Doping photocatalysts with various elements is a widely spread practice for improving photocatalytic properties at the expense of widening the absorption area of the sun radiation [62]. When considering items of biological origin as precursors, it is necessary to conduct a quality analysis and assessment of the concentration of the doped elements in their composition. Figure 3b presents the XRF analysis results that show the presence of the following elements in grinded clam shells: Na, Mg, Al, Si, P, S, K, Ca, Fe, and Sr. The elemental composition of the clam shells under study can be classified into four groups according to a possible appearance of the given elements in the shell composition: 1—milling agents' material; 2—material of natural minerals of sea bottom and coastal discharge area; 3—seawater ion content; and 4—material of organic nature. The highest value of the mass concentration in all the shells under study and reference standard falls on Ca and equals about 55% of the sample weight. The cumulative mass

content of the doped elements in the samples and the reference sample are distributed as follows: *Crenomytilus grayanus*—0.805%; *Callista brevisiphonata*—1.010%; *Mizuhopecten yessoensis*—1.027%; and  $\text{CaCO}_3$ —0.237%. The mass concentrations of the elements Al, Mg, and Fe in all the samples under study are in equal amounts (0.02–0.10%), which might be indicative of their appearance in the result of pollution with grinding and milling agents during the process of sample preparation. However, the appearance of the given elements may also be explained by the exposure to natural factors (contact with sea bottom and coastal area minerals) and conditions of the animals' habitat (seawater ion content). Such elements as Ca, Sr, Na, and K are those of the most frequent cations that enter the seawater composition [63]. The content of Sr and Na in the test portions of the samples under study exceeds 0.1%, which may be related to the appearance of such elements in the clam shells' composition during their lifetime in seawater. The mass concentration of K is minimal for all the samples under study and is at the level of the XRF method's ultimate sensitivity. The content of Si also exceeds 0.1% in all the samples under study and can be explained by the impact of silicon oxide on the shell in the process of friction on the sea sand bottom or the sand in the area of coastal discharges. In fact, clam shells also contain organic matters that serve reinforcement, protection, and cover functions [64]. The basic organic elements in the composition of clam shells are conchiolin protein [65], carbohydrates, lipids, free peptides, pigments, and other metabolites [66]. Protein molecules and organic matters binding them contain such elements as H, O, N, C, and S, P. According to the instrumental capabilities of the XRF method, the number of organic matters and their degree of preservation in the shells from coastal discharges may be assessed only by the elements with an atomic number over 10, such as S and P. The highest content of the elements characterizing the organic matter is observed with *Mizuhopecten yessoensis*. This fact might be explained by a better preservation of organic molecules exposed to environmental factors due to the anatomic peculiarities of the shell structure and a large size of the shell *Mizuhopecten yessoensis* compared to *Callista brevisiphonata* and *Crenomytilus grayanus* (Supplementary Figure S2). On the other hand, sulfate anion is also one of the most frequently found seawater anions [66], thus complicating the assessment of the organic origin of sulfur in the framework of this study. Considering the elemental composition of the materials under study in terms of their toxicological hazard to humans, the tests conducted showed the presence of one element only (Sr) in the clam shells' composition which has a negative effect on human metabolism and is the subject of debate at present [67]. On the other hand, Sr is both a perspective component of solar photocatalysts [37] and a highly effective dopant UV photocatalyst [68]. Thus, the utmost importance should be placed on observing the rational balance between the toxicological safety and water treatment efficiency of applied photocatalytic materials. The presence of doping elements in all the shells under study in the amount of less than 1% and the absence of elements highly toxic to biological objects (Figure 3b) substantiate the high bio-indifference of the materials under consideration in the paper for water treatment photocatalytic applications. The analysis of certain particles in grinded powders of clam shells through the EDX method also showed the absence of elements hazardous to water ecosystems and biological objects (Supplementary Figure S3).

### 2.3.2. Organic Composition

Clam shells have a layered structure, and, generally, three layers can be distinguished: external (periostracum)—protective and exposed to the marine environment; middle—serving a mechanical function; and inner layer (pearl layer)—serving a lining and forming functions. When considering clam shells as powder material for photocatalytic applications (Figure 1), the largest number of organic matters obviously may come from the middle layer due to its greatest thickness. In using clam shells as carriers of photocatalytic coating and assessing their sorption activity, the testing for the presence of organic impurities in the external and inner layers is important. The evaluation study of the presence of organic impurities in clam shells compared with the reference sample of calcium carbonate is shown in Figure 4. According to the data introduced, the common motive of all

spectra corresponds to the IR spectrum of calcium carbonate, which speaks for the fact that inorganic components dominate in the clam shells from coastal discharges. Nevertheless, according to the data [64], the protein component in clam shells may be preserved for a longer time and serves as a time marker in geological investigations. The peak of bands' vibrations presented in the FTIR spectra (Figure 4) can be divided into three groups: 1—peaks corresponding to bands vibrations in calcium carbonate (2980, 2878, 2510, 1800, 1440, 872, 847, 712, and 700  $\text{cm}^{-1}$ ); 2—peaks corresponding to bands' vibrations in organic structures and water (3600–3000, 2925, 1440, 1082, and 830  $\text{cm}^{-1}$ ); 3—hard-to-identify peaks or peaks corresponding to vibrations of various bands between various elements (2980, 2878, 2510, 1800, 1440, 1160, 1082, and 1020  $\text{cm}^{-1}$ ). The vibrations ranging from 3600 to 3000  $\text{cm}^{-1}$  correspond to vibrations of hydrogen in organic compounds with such functional groups as  $-\text{N}-\text{H}$  and  $-\text{O}-\text{H}$  [69–71], as well as to vibrations of hydrogen in the molecules of adsorbed water [72,73]. According to Figure 4, all of the layers and powders of clam shells under study have a wide peak of vibrations in the area under consideration, which may count in favor of the presence of organic impurities. However, the wide peak in the area of 3600–3000  $\text{cm}^{-1}$  does not make it possible to exactly identify the presence of vibration peaks of  $-\text{N}-\text{H}$  groups of 3280–3292  $\text{cm}^{-1}$  [71], and, due to the aquatic habitat of clams, the peak under consideration may belong to the absorbed water. The vibration peak around 2980  $\text{cm}^{-1}$  is observed in all the samples under study and might belong to the bands' vibrations in the calcium carbonate structure that are hard to identify according to the literature references. The peak of vibrations around 2925  $\text{cm}^{-1}$  is observed both in the external and inner layers of the clam shells under study and corresponds to the basic structural element of organic molecules  $-\text{C}-\text{H}$ , according to the data [65,69]. At the same time, this peak is poorly noticed or completely absent in the powder samples (Figure 4). It may speak for a smaller thickness of the external and inner layers, containing organic impurities that are equally distributed in the powder in grinding and become hypersensitive to the FTIR method. The peak of vibrations around 2878  $\text{cm}^{-1}$  might belong to the second overtones for the widest peak of 1440  $\text{cm}^{-1}$  observed in the spectra of all the samples under study. According to the data [60,69,74], the peaks around 2510, 1800, and 1440  $\text{cm}^{-1}$  refer to the vibrations of the carbonate group and are present in all the samples under study. Due to the large width of the peak about 1440  $\text{cm}^{-1}$ , according to the data of various researches, the following interpretations are possible in respect to this peak belonging to the bands' vibration in 1455  $\text{cm}^{-1}$ —“ $\text{CaCO}_3$ ” [75]; 1440  $\text{cm}^{-1}$ —“calcite” [76]; 1472  $\text{cm}^{-1}$ —“ $\text{CO}_3^{2-}$ ” [60]; 1400  $\text{cm}^{-1}$ —“ $\text{C}-\text{O}$  from carbonate” [31,74]; 1420  $\text{cm}^{-1}$ —“bands of amide II” [77]; and 1396–1422  $\text{cm}^{-1}$ —“symmetric  $\text{COO}$ ” [71]. The represented data, to a greater extent, verify the affiliation of the peak around 1440  $\text{cm}^{-1}$  to the vibration of bands between carbon and oxygen in calcium carbonate. According to Figure 4, the group of peaks in the range of 1300–900  $\text{cm}^{-1}$  is completely absent in the calcium carbonate reference standard and may belong to the vibrations of bands in organic compounds preserved in the clam shells from coastal discharges. However, the analysis of the literature reference shows various interpretations of the affiliation of the peaks around 1160, 1082, and 1020  $\text{cm}^{-1}$  to the vibrations of bands between various elements. The peak of vibrations around 1160  $\text{cm}^{-1}$  is observed only with *Mizuhopecten yessoensis* in all the layers under study and the grinded powder of its shells (Figure 4). On the one hand, the peak of vibrations around 1151  $\text{cm}^{-1}$ , according to the data [71], corresponds to the vibrations of bands of “ $\text{C}-\text{O}-\text{C}$  of carbohydrate”; however, the wide peak around 1160  $\text{cm}^{-1}$  and the difference of 9  $\text{cm}^{-1}$  cast some doubt on the affiliation of the given peak to an organic component. On the other hand, according to the data [77], the peak of vibrations around 1157  $\text{cm}^{-1}$  corresponds to the bands' vibrations in phosphates. Such an interpretation correlates well with the earlier conducted tests of the elemental composition (Figure 3b). According to the test data, the largest amount of phosphorus was specifically found in the *Mizuhopecten yessoensis* shells. The peak of vibrations around 1082  $\text{cm}^{-1}$  is observed in the shells of all clams under study and, to a greater extent, is revealed with *Callista brevisiphonata*, in the shell of which the content of aragonite is maximal (Figure 3a). The lowest intensity of this

peak is observed in the *Mizuhopecten yessoensis* samples, the content of aragonite in the shell of which is minimal. The effect of aragonite on the intensity of the peak around  $1182\text{ cm}^{-1}$  correlates well with the data [76] on the affiliation of the peak to the mode of aragonite. However, there are other data [73] on the affiliation of the peak  $1080\text{ cm}^{-1}$  to calcite which contradict the conducted tests that showed the absence of such a peak in the calcium carbonate reference standard fully consisting of calcite. On the other hand, the literature references show the affiliation of the peak around  $1082\text{ cm}^{-1}$  to vibrations of bands in such organic compounds as  $1082\text{ cm}^{-1}$ —"C-OH" [60];  $1073\text{ cm}^{-1}$ —"carbohydrates" [77]; and  $1069\text{--}1084\text{ cm}^{-1}$ —"C-O of carbohydrate or  $\text{SO}_3$  symmetric" [71]. In accordance with the above approaches to the identification of peak  $1082\text{ cm}^{-1}$ , it can be stated with high probability that this peak belongs to the vibrations between carbon and oxygen in calcium carbonate with the aragonite modification. The given statement is also confirmed by the high intensity of this peak in the grinded *Crenomytilus grayanus* shells that, by  $\approx 40\%$ , consist of aragonite (Figure 3b). Moreover, according to the data of Figure 4, the inner layer of the *Crenomytilus grayanus* shell is the richest in aragonite, while in the spectrum of the external layer, this peak is completely absent. The peak of vibrations around  $1020\text{ cm}^{-1}$  is clearly observed in the powder of the *Mizuhopecten yessoensis* shells and all of its layers; to a lesser degree, this peak was observed in the powder of the *Crenomytilus grayanus* shells and its external layer. In the *Callista brevisiphonata* samples, the peak under study is hard to discern. In accordance with the data [74], the peak around  $1020\text{ cm}^{-1}$  may belong to the vibrations of bands in ion hydro-phosphate, which correlates quite well with the elemental composition test (Figure 3b) and the relative distribution of phosphorus in relation to the clam shells under study. In the range of the waves' lengths from  $900$  to  $800\text{ cm}^{-1}$ , there are two peaks around the values of  $872$  and  $847\text{ cm}^{-1}$  that are typical for all samples and one peak around  $830\text{ cm}^{-1}$  present in the samples, but it is the reference sample of calcium carbonate. According to the data [69,75], peaks around  $872$  and  $847\text{ cm}^{-1}$  belong to the vibrations of bands between carbon and oxygen in calcium carbonate and are associated with calcite [73,76]. An important peculiarity of these peaks is their shift to a shortwave region upon the growth of the aragonite rate in the composition of the sample under study. According to Figure 4, a strong shift in these peaks in respect to the calcium carbonate reference standard is observed with the *Callista brevisiphonata* samples, with the absence of the peaks' shift characterizing the *Mizuhopecten yessoensis* samples consisting of  $\approx 90\%$  of calcite (Figure 3a). In the *Crenomytilus grayanus* samples, the shift of peaks  $872$  and  $847\text{ cm}^{-1}$  is observed for the powdered sample and inner-layer samples only. The external layer is characterized by the absence of the shift of these peaks, which may speak for the presence of calcium carbonate in the form of calcite in its composition. A similar trend in the peaks' shift depending on the aragonite content is observed for all the samples under study in respect to the peak around  $1800\text{ cm}^{-1}$ . The peak of the vibrations around  $830\text{ cm}^{-1}$  belongs to the vibrations of the "C-C stretch or CH bend" [71] and characterizes the presence of the organic matter preserved in clam shells. The highest intensity that the given peak has is in all the *Mizuhopecten yessoensis* samples. In the *Crenomytilus grayanus* samples, this peak is observed in the external layer only. The *Callista brevisiphonata* samples do not have such a peak on their spectra. The presence and intensity of the peak around  $830\text{ cm}^{-1}$  indirectly confirm a better preservation of the organic matter in the clam shells from the coastal discharges, or a larger number of the organic components in clam shells depending on the habitat or anatomic features. The vibration peaks around  $712, 700\text{ cm}^{-1}$  also belong to the vibrations of bands in calcium carbonate [69]; however, the peak  $700\text{ cm}^{-1}$  is only typical for the aragonite modifications [74]. According to Figure 4, the presence of the peak at  $700\text{ cm}^{-1}$  in all the samples under study is in strict compliance with the data from the X-ray diffraction analysis (Figure 3a). The absence of this peak in the external layer of *Crenomytilus grayanus* also confirms the earlier described data on the peculiarities of the peaks around  $1082, 872, \text{ and } 847\text{ cm}^{-1}$  and characterizes the composition of the external layer as calcite. Thus, the tests through the use of the FTIR method showed the presence both of organic and inorganic components in the composition of clam shells. The typical

peaks of vibrations in organic molecules showed that, depending on the clam species, a different ratio of the organic component to calcium carbonate is observed depending on the layer-wise buildup of clam shells. The completed tests confirm the necessity to assess the presence of the organic impurities in clam shells when they are used as materials for photocatalytic applications.

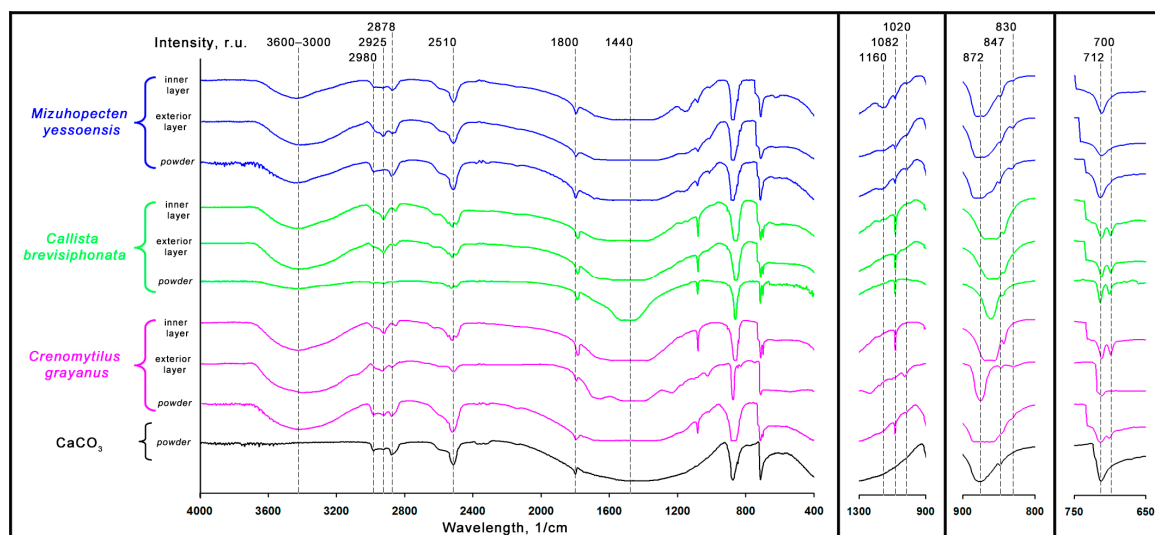


**Figure 4.** Comparative studies on FTIR spectra of different layers of mollusk shells and their crushed shells relative to the reference calcium carbonate.

### 2.3.3. “Powder-like” Morphology and Granulometric Properties

The material in the form of powder is one of the most common forms of use of substances in various technological processes. Powdered material is applied in photocatalyst investigations as a precursor for the synthesis of various photocatalysts or as a photocatalyst itself. The most important characteristics of powders are their granulometric parameters to specify the average diameter of particles,  $D$ ; specific surface of powder,  $S_s$ ; and modality of distribution of particles by size,  $Mod$ .  $S_s$  and  $D$  have a substantial effect on the process of the chemical synthesis of photocatalysts, as well as on physicochemical processes of sorption and decomposition of an organic matter upon photo-destruction. The  $Mod$  has an important significance upon the compaction of powders for the further receipt of volume photocatalytic materials with given porosity values. It is known that calcium carbonate does not show photocatalytic activity, and, for this reason, the powder material from clam shells is studied from the point of view of precursor matter for the synthesis of photocatalysts (Figure 1). The morphology and granulometric parameters of the grinded clam shells are represented in Figure 5. In all the grinded powders at  $500\times$  magnification, there can be identified three types of particles: (1) large spherical particles covered by smaller particles; (2) particles of intermediate size and of irregular form with chipped sides also covered with smaller particles; and (3) finely dispersed particles. The large spherical particles probably are the agglomerations formed due to absorbed water (Figure 4) from the finely dispersed particles during the storing of powders after grinding. The irregularly formed particles are a product of grinding the clam shells with layers and direct buildup (Supplementary Figure S1). These particles are well discerned on the SEM images of *Crenomytilus grayanus* at various magnifications. The presence of similar particles speaks in favor of a higher resistance of the *Crenomytilus grayanus* shells to impact loads compared to the shells of other clams under similar grinding conditions. According to the data of the LD method, the average diameter of particles for the grinded shells of *Crenomytilus grayanus* is the largest of all the powders under study and equals  $18.3\ \mu\text{m}$ . The SEM image ( $500\times$ ) of the *Mizuhopecten yessoensis* powder shows the absence of the large number of spherical agglomerates, unlike the powders of *Crenomytilus grayanus* and *Callista*

*brevisiphonata* (Figure 5). The low tendency toward agglomeration of the *Mizuhopecten yessoensis* powder might be explained by the presence of a larger amount of organic matter in clam shells. The earlier received data on XRF and FTIR (Figures 3b and 4) indirectly confirm the pieces of research [78] in grinding calcite with the present organic matters. On the other hand, according to the data of Figure 3a, the *Mizuhopecten yessoensis* shell consists of 86% calcite, for which the particles are probably, to a lesser degree, subject to agglomeration under the effect of absorption water than the aragonite particles entering the composition of the *Crenomytilus grayanus* and *Callista brevisiphonata* shells. According to the granulometric analysis, the grinding of clam shells in equal conditions shows multimodality on the histogram of the particles' distribution by size for all the samples. The common motive of the presented histograms (Figure 5) is the presence of about 50% in mass of the particles below 10  $\mu\text{m}$ , which speaks to the similarity of the grinding mechanism for all the samples under study. However, the different ratio of calcite to aragonite and the presence of a different number of organic impurities lead to the redistribution of maximum values of Mod on the presented histograms. The largest number of Mod on the histogram characterizes the *Crenomytilus grayanus* sample. According to the values of  $S_s$  and  $D$ , this sample is characterized by a higher resistance to impact loads during the grinding process, which is supported by a lower mass content of particles in the range from 0.01 to 0.1  $\mu\text{m}$  and a presence of an expressed Mod with particles around 100  $\mu\text{m}$ , in comparison to the grinded powders of *Mizuhopecten yessoensis* and *Callista brevisiphonata*. The smallest value of  $D = 6.6 \mu\text{m}$  and absence of the particles of over 50  $\mu\text{m}$  in size are typical for the *Mizuhopecten yessoensis* powder, which points out the high grindability of the shells of this clams. The *Callista brevisiphonata* powder has much lower values of the first two Mods (0.08 and 1.17  $\mu\text{m}$ ) on the distribution histogram in comparison to the histogram of the *Mizuhopecten yessoensis* powder probably due to the prevalence of aragonite ( $\approx 98\%$ ) in its structure. Because of a special crystallographic buildup, the aragonite crystals have an elongated columnar shape, which is more subject to destruction than a platy-cubic form for calcite crystals [79] (Supplementary Figure S1). The Mod with a maximum of 0.08  $\mu\text{m}$  in the *Callista brevisiphonata* sample may assumably be explained by the destruction of the end-parts of the aragonite columnar crystals in the perpendicular direction to the crystal growth. All the powders of the grinded clam shells under study have an expressed decline in the volumetric quantity of the particles in the range from 5 to 10  $\mu\text{m}$  (Figure 5). This effect is most characteristic of the powder of the grinded *Crenomytilus grayanus* shells. According to the data on the phase and elemental compositions (Figures 3 and 4), the effect of the smaller mass number of these particles correlates with the presence of the organic component remains and the ratio of calcite to aragonite. This correlation is well traced in the line of the *Crenomytilus grayanus*, *Mizuhopecten yessoensis*, and *Callista brevisiphonata* powders and shows the growth in the mass number of the specified articles with the growth in the amount of aragonite and decline in the number of organic impurities in the powders of the clams under study. On the other hand, the smaller number of particles of the specified range might be explained by the morphological peculiarities of the buildup of shells, where the structural elements have the dimensions of monolithic grains (of calcite/aragonite) of below 5–10  $\mu\text{m}$ . At the higher structural level, the monolithic grains have interfaces with various planes of the crystal growth, defects, or various ratios of reinforcing interlayers of the organic matter. In grinding conditions, the specified interfaces of grains may quickly be destroyed, enriching the powder with monolithic particles more resistant to grinding. A detailed study of the described dependency of grinding from the correlation of phases and morphological features of the shells' buildup was outside the scope of this paper. The study of the granulometric characteristics of the powders from clam shells showed that the *Mizuhopecten yessoensis* shells are the least resistant to grinding ( $S_s = 46,072 \text{ cm}^2/\text{cm}^3$ ), and the most resistant to impact loads turned out to be the *Crenomytilus grayanus* shells ( $S_s = 36,066 \text{ cm}^2/\text{cm}^3$ ). According to the distribution histograms, it is shown that are both the similar mechanisms and individual features of the process of grinding the shells of the

clams under study are traceable, which should be taken into consideration when using them as precursor substances for the synthesis of photocatalysts.

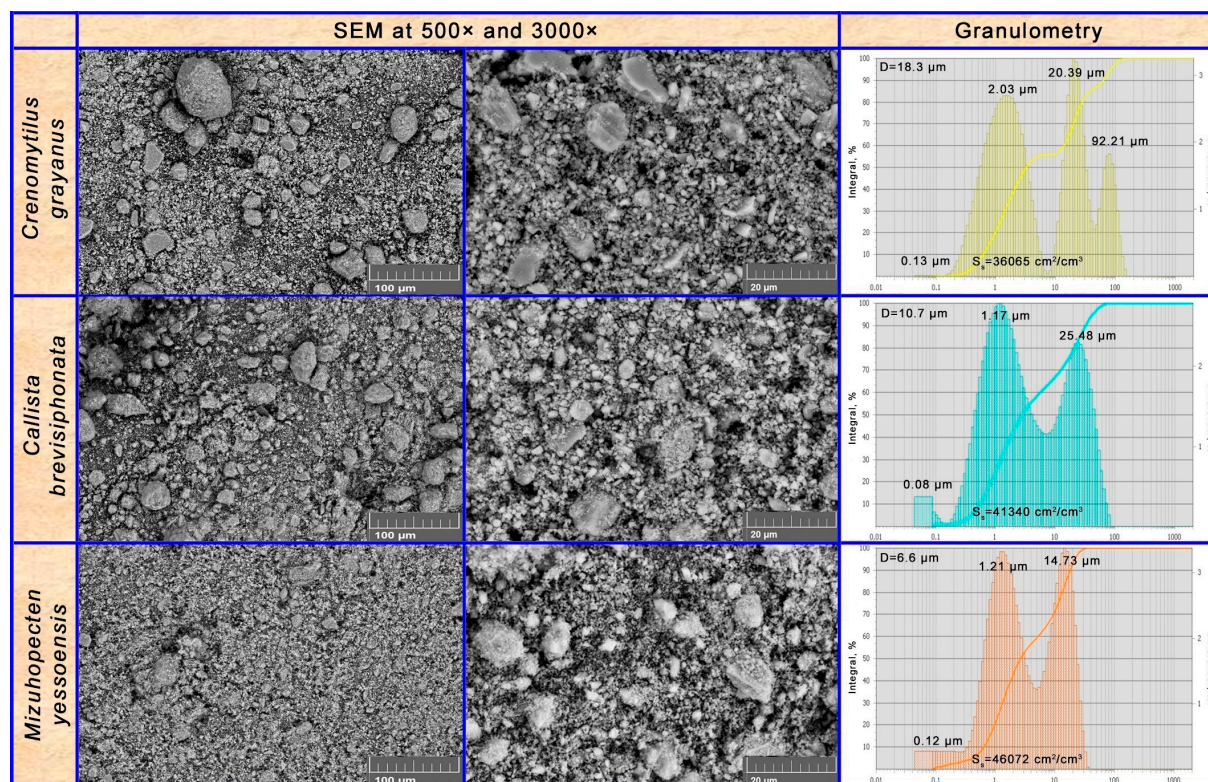


Figure 5. SEM images and histograms of particle size distribution for powders of grinded clam shells.

### 2.3.4. “Carrier-like” Mechanical and Functional Properties

High requirements are imposed on all types of carriers of various catalytic coatings with regard to their mechanical durability, chemical inertness, and properties of surfaces to be coated. In particular, additional functional requirements are set for the carrier of photocatalytic coatings, such as bio-indifference, wettability, and mechanical durability in closed-type photocatalytic water treatment plants with overpressure of the treated waters. The clam shells under study are initially characterized by a sufficient mechanical and hydrolytic resistance in a water medium with a high content of various ions (seawater), and also by the absence of bio-toxic elements in their composition. The mechanical durability of the clam shells, at their possible use as carriers of photocatalytic coatings in flow-through water treatment plants, was assessed according to the values of three-point flexural strength (Table 1) as a result of the biological peculiarities of the shells growth and formation, the samples for studying  $\sigma_f$  were prepared and tested according to the scheme (Supplementary Figure S1). According to the conducted studies, a common trend is traced for all the shells under study showing that within the error  $\sigma_{f(\perp)} > \sigma_{f(\parallel)}$ . This peculiarity is explained by the directed growth of grains of calcium carbonate at the shell’s formation during the clam life, and also by the respective direction of the binders of the organic matter grain (grains interface). The resistance to the applied load in the case of determining  $\sigma_{f(\perp)}$  is put up to a greater extent by the calcium carbonate grains, but at determining  $\sigma_{f(\parallel)}$ , the sample destruction takes place along the less mechanically durable interfaces of grains (reinforcing bond of organic component). By the highest values of  $\sigma_{f(\perp)}$  and  $\sigma_f$  are characterized the samples prepared from the *Mizuhopecten yessoensis* shells. This peculiarity can be explained by a most homogeneous phase composition (Figure 3a) of this clam shell and the presence of a sufficient number of reinforcing organic bond (Figure 4). The average value of the flexural strength of the samples from all the clam shells is within 3–4 MPa, which exceeds the used norms of pressure (0.03–0.5 MPa) in cold water supply piping (RUS-SNiP-2.0401-

85). When using whole clam shells as carriers of photocatalytic coatings, an important parameter is the common defectiveness of volume material, which was assessed by way of measuring strength to compression (Table 1). The *Mizuhopecten yessoensis* shell was characterized by the highest value of  $\sigma_c$ , which was 2.4 MPa. This shell durability exceeded the  $\sigma_c$  values of the *Crenomytilus grayanus* and *Callista brevisiphonata* shells by more than 4 times. The presence of expressed strengthening ribs with the *Mizuhopecten yessoensis* shell (Supplementary Figure S2), as well as a minimal number of macro-defects in the shell material mass, may serve as an explanation for this fact. The fact of the  $\sigma_f$  values exceeding the  $\sigma_c$  values for all the shells under study (Table 1) is also explained by the number of micro- and macro-defects in the mass of a whole shell and samples cut out of it (Supplementary Figure S1). When comparing the values of  $\sigma_f$  and  $\sigma_c$  of the studied shells with the resistance of the shells to impact loads at grinding (Figure 5), a contradiction can be stated that the material of the *Mizuhopecten yessoensis* shell has higher durability values, but, at the same, it better responds to grinding. However, with a more detailed consideration of this fact, it becomes obvious that the grinding degree ( $D, S_s$ ) depends on the presence of surface-active substances (organic component of shells) and the homogeneity of the phase composition, while mechanical strength depends on the number and mutual disposition of micro- and macro-defects in the structure of volume material. Consequently, making a direct correlation between the values of ( $D, S_s$ ) and ( $\sigma_f, \sigma_c$ ) is not correct.

**Table 1.** The mechanical properties of mollusk shells.

	Flexural Strength, MPa			Compressive Strength, MPa	Density, g/cm <sup>3</sup>	Porosity, %
	$\sigma_f(\parallel)$	$\sigma_f(\perp)$	$\sigma_f(\text{Average})$	$\sigma_c$	$\rho$	$\phi$
<i>Crenomytilus grayanus</i>	3.38 ± 0.43	3.56 ± 0.58	3.47	0.75 ± 0.23	2.65 ± 0.05	6.69
<i>Callista brevisiphonata</i>	1.67 ± 0.35	4.34 ± 0.46	3.00	0.80 ± 0.31	2.72 ± 0.01	6.88
<i>Mizuhopecten yessoensis</i>	3.04 ± 0.28	4.97 ± 0.86	4.00	2.36 ± 0.57	2.66 ± 0.01	2.91

Porosity can be referred to as a parameter comprehensively characterizing the presence of macro- and micro-defects. The  $\phi$  parameter for all the shells was studied based on the data of the mass ratio of calcite to aragonite (Figure 3a), material hydrostatic density (Table 1), and densities of calcite (2.71 g/cm<sup>3</sup>)/aragonite (2.93 g/cm<sup>3</sup>) according to Equation (4). According to the lowest porosities, we characterized the samples of the *Mizuhopecten yessoensis* shells, which correlate with the maximum values of  $\sigma$  and indirectly confirm the number of micro- and macro-defects in the shells of this clam. The  $\rho$  value in the current paper was studied also to receive reference data that can be used in the creation of photocatalyst materials based on the shells of mollusks drifting in the subsurface layer (Figure 1). The elaboration and study of such materials were not intended as the tasks of the current paper. The geometric features of the carrier of photocatalytic coating play an important role both in the efficiency of the photocatalyst absorbing solar light and the processes for creating coatings through various computerized programmed methods (laser processing, spray coating, ion deposition, etc.). The carrier's symmetry and the camber degree of its functional surfaces also influence the compactness of the photocatalyst material packing both upon its transportation and its use in open-type water treatment plants (Figure 1). The assessment of the camber degree of the prospective carriers of photocatalytic coatings is represented on Figure 6 in the form of upper, lateral, and front planes of the clam shells under study. According to Figure 6, the upper projections of the *Crenomytilus grayanus* and *Callista brevisiphonata* shells are close to ovals by form. The one that is the most symmetrical and closest to the shape of a circle is the *Mizuhopecten yessoensis* shell. The lateral and front projections are generally characterized by the shift of the highest point of the shell in respect of the mid-length of the projection under consideration. The consideration of the species features of shells is important for an effective photocatalytic coating through various methods and shall be justified by the choice of the shells with the

highest number of symmetric projections of their planes. Of all the studied clam shells, the *Mizuhopecten yessoensis* shell has the most proper form to be used as a carrier of photocatalytic coatings. From the point view of an effective illumination with the sunlight of the shells used as carriers, it is advisable to put the coating on the arched (uppermost) side of shells (Supplementary Figure S2). Other important properties of the carriers of photoactive materials are the physicochemical properties of their surface.

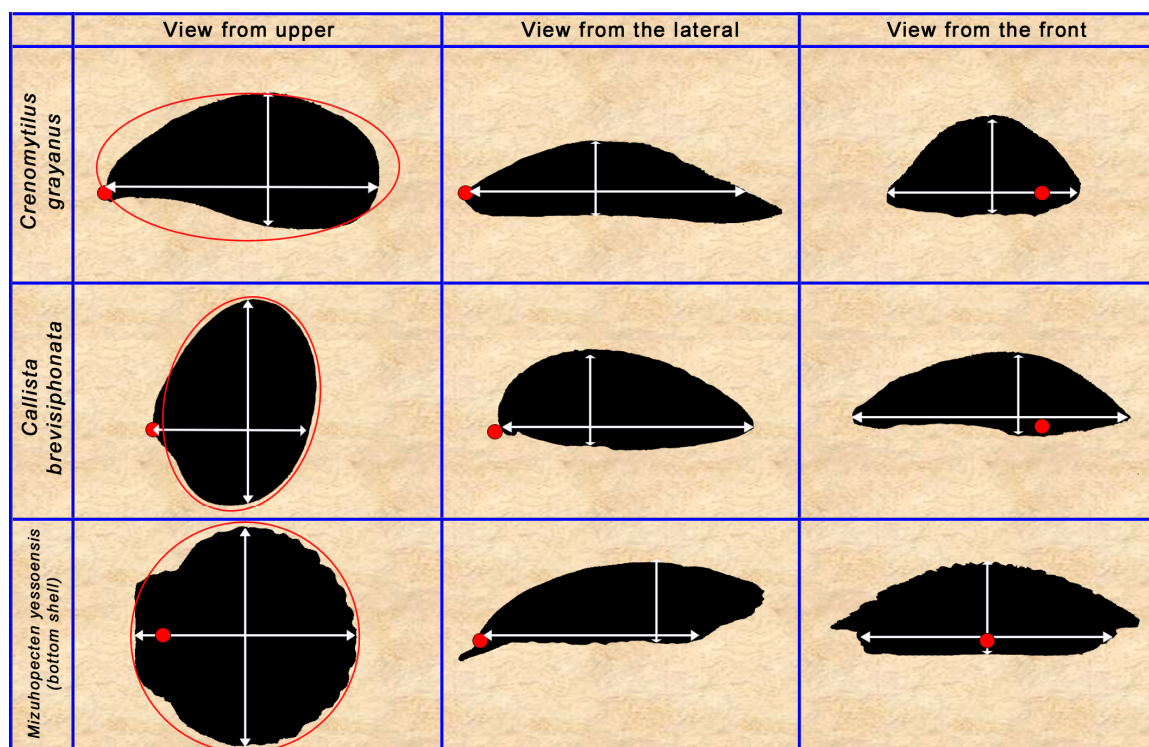


**Figure 6.** Projections of mollusk shells: upper, lateral, and front planes. The red circle is the location of the top of the shell (the starting point of growth).

The occurrence in water medium of various physicochemical processes on the surface both of carriers and photocatalytic materials influences the efficiency of water treatment. The ability of water to wet the surface of the material has a substantial effect on the sorption processes at the photooxidation of substrate both in the conditions of simulation tests of photocatalysts and industrial water treatment plants. The choice of the segment of the carrier's surface for coating shall also be justified by the surface properties. The creation of a photocatalytic coating on clam shells is possible on three surfaces: (1) external layer (periostracum), (2) abrasive/grinded-off middle layer (Ostracum), and inner layer (Pearl layer). The ability of water to wet such surfaces was studied through the use of CA (Figure 7). According to Figure 7, all of the studied surfaces for each shell have a CA below  $90^\circ$ , which proves good wettability. Depending on the mollusk species, the external layer is lined with organic matters of various thickness and morphology (Supplementary Figure S2). This feature is most obviously expressed with the *Crenomytilus grayanus* shells, and the layer under study has the highest CA, equal to  $53^\circ$  (Figure 7a). This layer might service the protection function and be characterized by an enhanced capability to shed seawater. The external layer of the *Callista brevisiphonata* and *Mizuhopecten yessoensis* shells has a CA about  $35^\circ$  due to a various degree of the surface roughness and a lower content of organic matter comparing to *Crenomytilus grayanus* (Figure 7a,d,g). The studies of the CA of a middle layer of clam shells (Figure 7b,e,h) showed the lowest values ( $\approx 10^\circ$ ) for the layers of *Crenomytilus grayanus* and *Callista brevisiphonata* compared to the CA =  $48^\circ$  of the middle layer of *Mizuhopecten yessoensis*. These differences are explained by the preparation of the middle-layer surface for each of the studied shells. At the first stage, we checked the

ability of shells to split into layers parallel to the growth line from the shell top to its side under an impact of little effort. Only the *Mizuhopecten yessoensis* shells were subject to layer separation, and the CA was measured on the surface of one of such layers, which was not subject to additional mechanical treatment. The morphology of such a layer (Figure 7h) is close by its roughness degree to the inner layer of *Mizuhopecten yessoensis* (Figure 7i), and the CA values were equal to 48° and 45°, respectively. On the other hand, the *Crenomytilus grayanus* and *Callista brevisiphonata* shells did not reveal the capability for layer separation and were subject to abrasive mechanical treatment to study the morphology and CA of the middle layer. According to the SEM data, on the surface of the middle layer of the samples (Figure 7b,e), the longitudinal grooves of from the abrasive material are observed, along which the water drop quickly spread, which accordingly explains the minimal values of  $CA \approx 10^\circ$ .

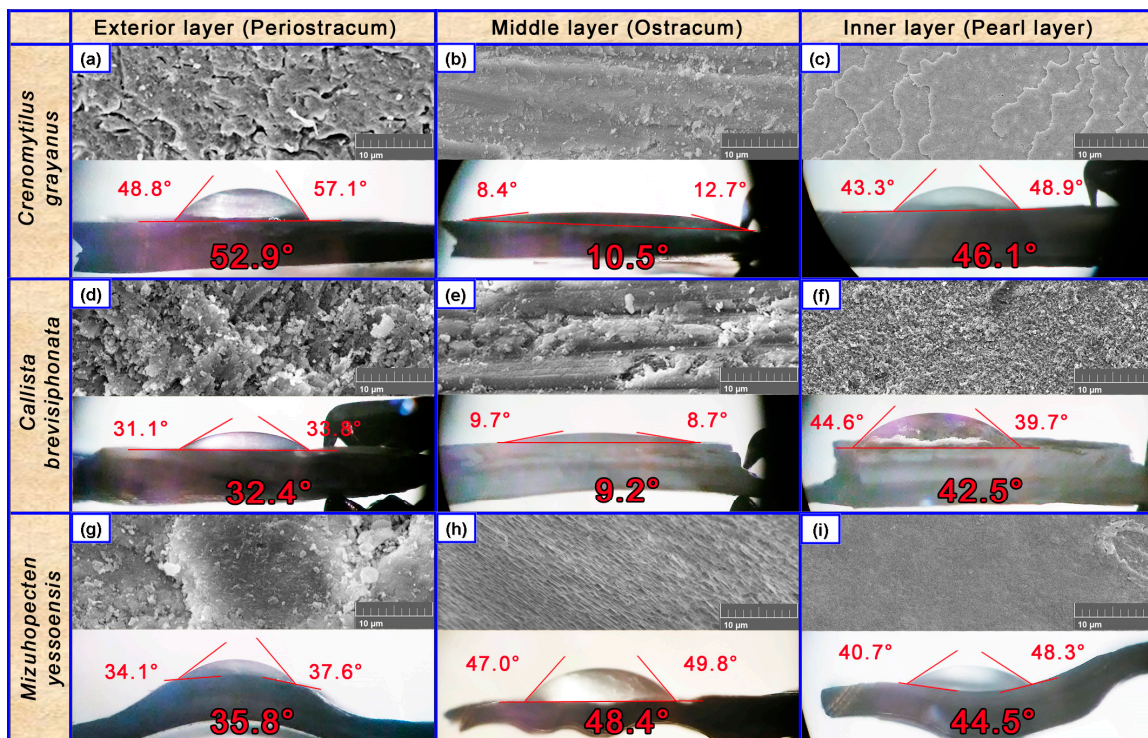


**Figure 7.** Surface morphology of different shell layers and CA values. *Crenomytilus grayanus*: (a) exterior layer (b) middle layer (c) inner layer. *Callista brevisiphonata*: (d) exterior layer (e) middle layer (f) inner layer. *Mizuhopecten yessoensis*: (g) exterior layer (h) middle layer (i) inner layer.

The study of the CA of the inner layer of shells (Figure 7c,f,i) showed an approximately similar value for wetting these surfaces with water. The layer adjacent to the visceral organs of mollusks has a low roughness and, according to the FTIR spectroscopy data (Figure 4), has an organic component most clearly expressed with *Crenomytilus grayanus* and *Mizuhopecten yessoensis*. The organic component serves lining and reinforcing functions in the shell's composition. A smaller amount of or disturbing the integrity of the organic component leads to the weakening of the calcium carbonate grains and to a respective growth of the surface roughness, as is in the case with the inner layer of *Callista brevisiphonata* (Figure 7f).

The species features of the formation of shells of various mollusks or the impact of environmental factors on the quantity and preservation of the organic component in the composition of various layers (Figure 7) directly effects the value of wetting characterized by CA. An increase in the wettability of the surface of the shells' layers with water happening along with its roughness increase is a characteristic that is revealed regularly. The roughness value of the carrier's surface has an important meaning for such methods of

adding photocatalytic coating as combining the carrier and photocatalyst powder by means of using an intercalary cementing layer [40]. The conducted CA studies also supported the prospects of preliminary mechanical treatment of the shell surface to make it rougher, remove layers of organic matter with low adhesion, and increase wettability. Putting coating based on water solutions of the photocatalysts' precursors on a good-wettability surface of a carrier may facilitate an effective chemical synthesis of the photocatalytic coating components and their effective adhesion. Good wettability of a carrier's surface is also able to improve the processes of transportation (sorption) of pollutants to the surface of the photoactive coating.

### 2.3.5. Sorption Activity

Sorption processes directly influence the efficiency of photooxidation of organic molecules on the surface of photocatalytic coatings. When on the surface of a photocatalyst or carrier placed in water, there is an electric charge opposite to the charge of the ionized part of the organic pollutant molecule, and it has a positive effect on the sorption process and, respectively, on the photooxidation efficiency. The chemical inertness and hydrolytic stability of a carrier's material must also ensure that organic pollutants are not destroyed by a non-photocatalytic mechanism both under model test conditions and under conditions of applying photocatalytic materials in industrial water treatment systems. The S/PhSA studies of clam shells, both in the form of powder and a plate cut out of a whole shell, in respect to four representatives of various classes of organic dyes (model pollutants), are represented on Figure 8. At the first stage of the experiment, comparative studies were conducted on the sorption activity and chemical interaction of the powder material of shells and the reference calcium carbonate (reference standard) with dyes at 20 °C and 50 °C in the dark to reveal the pattern of influence of the phase composition and organic component of shells on the described physicochemical processes. It is shown that the largest change in concentration was observed with the MG dye in the experiments with all powders of shells and calcium carbonate both at 20 °C and 50 °C. (Figure 8a,c,e). It is worth noting that the dyes' concentration was determined according to a decline in the optical density of their solutions (the solution color lightening) through the photometric method. It is known that many organic dyes are able to change their color in the medium with different pH values, herewith being acid–base indicators. On the other hand, the additional experiments showed that the powder of calcium carbonate dispersed in water has a weakly alkaline reaction of the  $\text{pH} = 7.9 \pm 0.1$  medium. The check of the hypothesis about the change in the color of MG upon interaction with a solution of calcium carbonate due to the influence of the pH of the medium was verified both by additional experiments with alkali solutions of similar pH values and by the data of the reference literature [50]. Raising the temperature of the calcium carbonate powder solution up to 50 °C raised the mobility of ions in the solution, which facilitated a more effective chemical interaction of MG with hydroxide ions (Figure 8a,c,e). Additional experiments on the effect of the solution with  $\text{pH} \approx 8$  on the color of MB, R6G, and MO did not reveal a significant decrease in the optical density of these dyes, and the interaction with the powders of calcium carbonate under study was further considered as sorption. According to the tests conducted at the dark stage at 20 °C, it was found that the dye most prone to sorption on the surface of the powders under study was MB. The MO dye, within the error, did not reveal the ability to sorption on the surface of all the powders under study. Among all the dyes under study, only MO in the solution is in the form of a negatively charged anion (Table 2). The absence of the MO sorption may indirectly indicate the presence of a negative charge on the surface of the powders of calcium carbonate under study, while the MB and R6G cations reveal some sorption activity. The lower values of the change in concentration with the cation R6G dye in comparison with MB may be contingent upon the larger geometric size of the R6G molecule (Table 2) and, respectively, a greater spatial difficulty of attracting the cation of the molecule to the charged centers of the surface of all the powders under study (Figure 8a,c,e). The studies of the sorption activity at the dark stage at 50 °C revealed obvious patterns of the decline

in the sorption activity of cation dyes (except for MG) by increasing the rate of thermal motion of molecules in the solution. In the framework of the conducted tests, it was not possible to identify a clear pattern of the effect of the ratio of calcite to aragonite on the sorption activity of shell powders in relation both to cationic and anionic organic dyes. However, the sorption activity of the *Mizuhopecten yessoensis* powder in respect to MB and R6G was higher than of other shell powders and reference standard consisting of calcite. This pattern may indicate the influence of impurities of the organic component (Figure 4) on the sorption processes by means of the *Mizuhopecten yessoensis* powder. At the second stage of the experiment, comparative studies were conducted on the interaction of the materials of shells powder and the reference calcium carbonate with dyes at 20 °C under the effect of simulated solar radiation to reveal the photocatalytic or photosorption activity of the materials under consideration. According to the data on the self-decomposition of dyes in the absence of powders under light radiation at 20 °C, MG and MB turned out to be less resistant to self-decomposition, with higher resistance to self-decomposition being revealed by MO and R6G. The studies showed that powders of all the shells, including of the reference standard, did not show photocatalytic and photosorption activity (Figure 8).

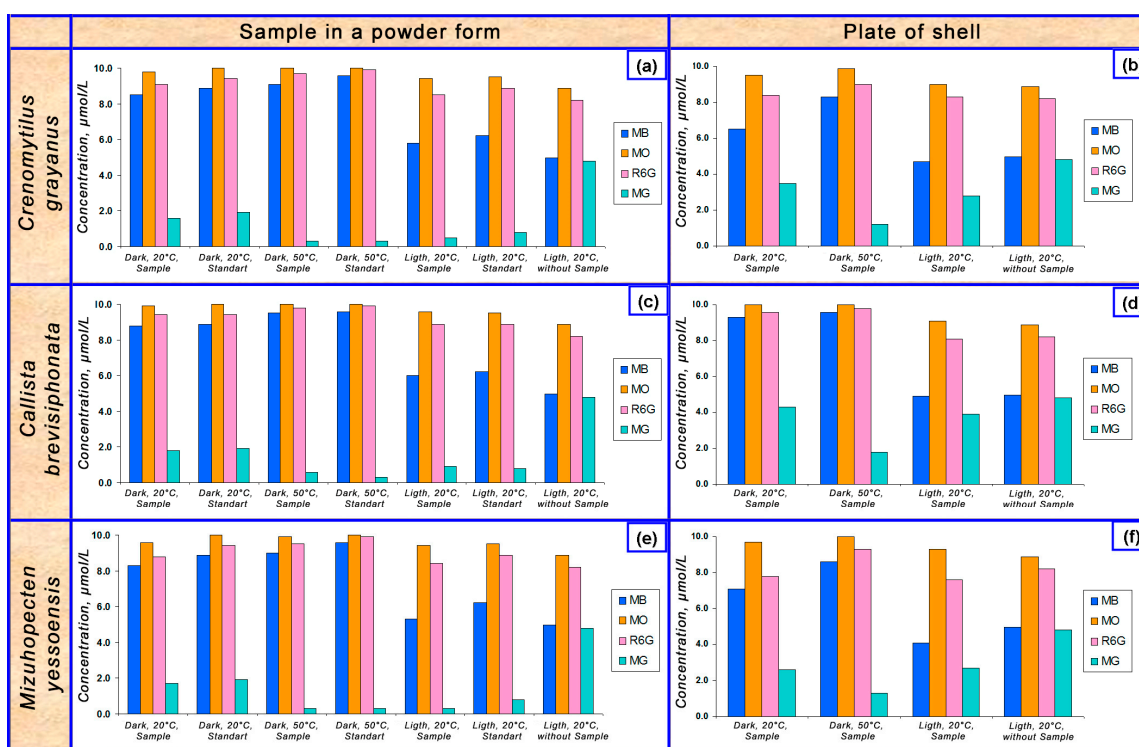


**Figure 8.** Sorption and photosorption activity of grinded and whole mollusk shells. *Crenomytilus grayanus*: (a) sample in a powder form (b) plate of shell. *Callista brevisiphonata*: (c) sample in a powder form (d) plate of shell. *Mizuhopecten yessoensis*: (e) sample in a powder form (f) plate of shell.

The decrease in concentration from the initial value for all the dyes under study in the presence of powders had smaller values than in similar conditions of the self-decomposition experiments. This pattern is explained by the dimming of the dyes solution by a dispersed powder not having photocatalytic activity, which reduces the rate of self-decomposition of the dye under the effect of light radiation. It is also shown that the powders under study do not have photosorption activity due to the fact that the decrease in the concentration of MB, MO, and R6G in the light and in the presence of powders was less than in the case of experiments in the self-decomposition of dyes. The decrease in the MG concentration in the presence of light and in the presence of powders to a greater extent than in the experiment with self-decomposition is explained by the total effect of the MG color-change processes at  $\text{pH} > 7$ , as well as by the self-decomposition of the dye under the action of light. The tests

of the sorption and photosorption activity of the plates from whole clam shells showed similar a dependency of the decrease in concentration of the dyes under consideration in respect of each other and in the experiment with powders (Figure 8b,d,f). However, a distinctive feature of the plates was the preservation of the external and inner layers of clam shells that, due to the presence of the organic component, revealed a higher sorption activity than the similar powders in equal experimental conditions. The conducted tests showed the importance of taking into account sorption activity and chemical inertness when choosing a carrier material for photocatalytic coatings.

**Table 2.** Characteristics of the studied organic dyes (model organic pollutants) [80,81].

Name of the compound, CAS	Methylene blue CAS: 61-73-4	Methyl orange CAS: 547-58-0	Malachite green CAS: 2437-29-8	Rhodamine 6G CAS: 989-38-8
Class	Acridines	Azo Dyes	Arylmethane Dyes	Xanthenes
Chemical structure depiction				
Molecular weight, g/mol	319.9	327.3	364.9	443.6
The charge of the organic part of the molecule	cation	anion	cation	cation
Solubility in water, g/L at 25 °C.	0.043	0.200	40	1-5
Safety and hazards	 Corrosive	 Acute Toxic	 Corrosive	 Environmental Hazard
Toxicity LD50(rat), mg/kg	1180	60, oral	275, oral	debated
Number of publications on photocatalytic applications (Since Direct 1998–2022)	>13,000	>9000	>1500	>1100

### 2.3.6. Example of Practical Use

The shell of a bivalve mollusk, *Mizuhopecten yessoensis*, was chosen as a carrier of the photocatalytic coating (Figure 9).

Preliminary studies have shown that the shell of this mollusk is the most promising as a carrier of photocatalytic coatings due to the (1) uniformity of the phase composition (Figure 3a), (2) minimum content of impurities of other elements (Figure 3b), and (3) high mechanical strength of the shell (Table 1) and resistance to laser exposure. The image and morphology of the resulting coating is shown in Figure 9a. An analysis of the phase composition of the starting components and the resulting photocatalytic coating is shown in Figure 9b. According to phase analysis data, the shell of *Mizuhopecten yessoensis* consisted of calcium carbonate only in the crystallographic modification—calcite. Titanium oxide powder annealed at 900 °C also contained only one crystallographic modification—rutile. The study of the phase composition and photocatalytic activity of the resulting coating was carried out after preliminary separation of the coating from the shell and its subsequent grinding to a powder state. The synthesized coating contained two phases of calcium titanate—Ca<sub>3</sub>(Ti<sub>2</sub>O<sub>7</sub>) and CaTiO<sub>3</sub> (Figure 9b). Comparative studies of the photocatalytic activity of the coating and its starting components are presented in Figure 9c. It was shown that the powder from the mollusk shells does not have photocatalytic activity, while the powder from the resulting coating shows high photocatalytic activity compared to its original components (Figure 9c). The conducted research shows the fundamental possibility of obtaining photocatalytic materials based on bivalve mollusk shells. Detailed studies

of the photocatalytic materials obtained in this work (optical properties, phase and cyclic stability, etc.) will be the subject of our further research.

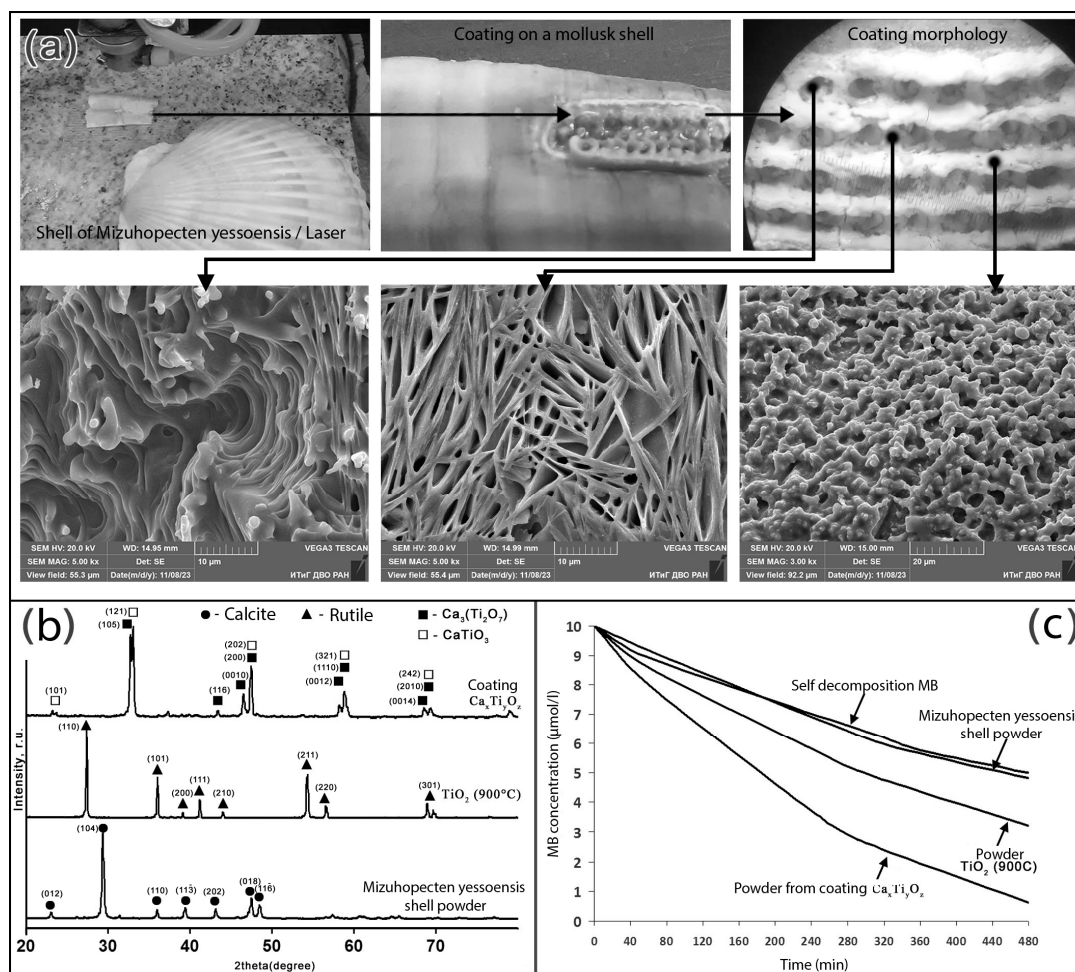


**Figure 9.** Structure and morphology of the coating (a), phase composition (b), and photocatalytic properties (c).

### 3. Materials and Methods

#### 3.1. Description of Initial Substances

Calcium carbonate (CaCO<sub>3</sub>)—GOST 4530-76, RUS was used as a reference standard to determine the following: (1) mass concentration of calcite at X-ray phase analysis of clams; (2) peaks of functional groups of organic compounds at IR spectroscopy of grinded clam shells, as well as internal and external layers of whole shells; and (3) sorption activity of grinded clam shells in respect to various types of organic dyes. The sorption activity was studied with the use of organic dyes: methylene blue (MB)—TU 2463-044-05015207-97, RUS; methyl orange (MO)—TU 6-09-5171-84, RUS; rhodamine 6G (R6G)—TU 6-09-2463-82, RUS; and malachite green (MG)—TU 6-09-1551-77, RUS (Table 2). Deionized water was received in the UPVA 4.1 unit (device for receiving water for lab analysis) and had an electric resistance of 16.6 MΩ.

#### 3.2. Description of the Analysis Methodologies

The samples were investigated using X-ray diffraction (XRD), using a Rigaku Mini Flex II diffractometer with CuKα ( $\lambda = 1.5406 \text{ \AA}$ ). The mass concentration in phases ( $\omega$ ) was determined via the procedure followed by [82], through the use of calcium carbonate as the reference standard, with 99% content of calcite. The X-ray fluorescence (XRF) elementary analysis of samples was conducted on the Bruker S4 Pioneer device. Energy-dispersive

X-ray (EDX) analysis and scanning electron microscopy (SEM) of the samples were studied with a Vega3 Tescan. The granulometric properties of powder-like samples were studied via the method of laser diffraction (LD), through the use of Analysette 22 MicroTec Plus, FRITSCH, within the range from 0.08 to 2000  $\mu\text{m}$ . We studied the modality of granulometric distribution (Mod), average diameter of powdered samples by Brouckere (D), and also the values of specific surface ( $S_s$ ). The study of the functional groups of organic compounds entering the composition of the mineral skeleton of the animals under study was conducted by means of Fourier-transform infrared spectroscopy (FTIR) of the device of Shimadzu IRAffinity-1 within the range from 400 to 4000  $\text{cm}^{-1}$ . The analysis of samples was conducted in KBr matrix at the mass ration of 1:30, respectively. The grinding of shredded fragments of the mineral skeleton of the studied animals was conducted in the Herzog HSM 100 disc-mill at the ratio of the mass of samples to the mass of milling agent, i.e., 1:200, for 1 min. The materials of shredding and milling agents contained elements of W, Co, C, and Fe. The contact angle (CA) of wetting for the tested samples was studied through the use of the MPCU-1 Lomo optical system by means of the Panasonic HC-VX980 video camera in the first second of the water touching the shells' surface. The volume of the deionized water drop was equal to 8  $\mu\text{L}$  and was dosed by using Biohit Proline 2–20  $\mu\text{L}$  at 25  $^\circ\text{C}$ . The calculation of the wetting angle was conducted with the help of specialized software for the right and left sides of the water drop photo image. CA was studied for internal and external sides of the mineral skeleton samples, as well as for the polished surface of the middle layer. The three-point flexural strength ( $\sigma_f$ ) of the mineral skeleton samples was studied by using the Nordberg N3610 hydraulic hand press according to the Equation (1) [GOST 8462-85, RUS]:

$$\sigma_f = \frac{3PL}{2ah^2} \quad (1)$$

where  $P$  is the highest load established at sample testing (kgf),  $L$  is the distance between axes of lower supports (m);  $a$  is the sample width (m), and  $h$  is the sample height at mid-length (m). The fracture test of the samples shells was performed by applying loads parallelly,  $\sigma_f(\parallel)$ , and perpendicularly,  $\sigma_f(\perp)$ , to the shell's plane of growth in the direction from its peak. The  $\sigma_f$  values introduced were the arithmetic mean in a series of 3 experiments with the shells of a single species, from where there were cut out 3 samples of each according to the scheme (Supplementary Figure S1). The compressive strength ( $\sigma_c$ ) of whole clam shells was studied through the use of the Nordberg N3610 hydraulic hand press according to Equation (2) [GOST 8462-85, RUS]:

$$\sigma_c = \frac{P}{S} = \frac{P}{0.5 \cdot (S_t + S_b)} \quad (2)$$

where  $P$  is the highest load established at sample testing (kgf); and  $S$  is the area of transverse section of sample calculated as the arithmetic means of areas of its upper ( $S_t$ ) and lower ( $S_b$ ) surfaces, taking into consideration a subtraction of an empty space area inside a shell. Due to the spherical shape of shells, the  $S_t$  value tends toward zero and is not used in the calculations. The  $S_b$  value was calculated with due consideration of the shell's thickness ( $h$ ) and a measured area of the shell's bedding ( $S_m$ ), according to Equation (3):

$$S_b = S_m - \pi \cdot \left( \sqrt{\frac{S_m}{\pi}} - h \right)^2 \quad (3)$$

The  $\sigma_c$  value introduced in the work was the arithmetic mean in the series of 6 experiments with the shells of the same species (Supplementary Figure S1). The determination of the density ( $\rho$ ) of fragments of the mineral skeleton of the animals under study was performed via the hydrostatic method, using Vibra AJ 220CE digital scales. The  $\rho$  values presented in the work were the arithmetic mean in a series of 6 measurements of the sam-

ples cut from a clam shell of each species. The porosity value ( $\phi$ ) was determined based on the data on  $\rho$ ,  $\phi$ , and densities of pure phases (calcite, aragonite) according to Equation (4):

$$\phi = \left( 1 - \frac{\rho \cdot (\rho_A \cdot \omega_C + \rho_C - \rho_C \cdot \omega_C)}{\rho_A \cdot \rho_C} \right) \cdot 100\% \quad (4)$$

where  $\rho_C$  is the density of calcite (2.71 g/cm<sup>3</sup>),  $\rho_A$  is the density of aragonite (2.93 g/cm<sup>3</sup>), and  $\omega_C$  is the mass ratio of calcite. The sorption and photosorption activity (S/PhSA) of grinded and solid samples were studied in the conditions typical to three cases of the most frequent photocatalytic applications: (1) dark sorption/desorption activity at 20 °C, (2) dark sorption/desorption activity at 50 °C, and (3) light sorption/desorption activity at 20 °C. The sorption/desorption activity of powders and solid samples was studied for each organic dye (MB, MO, R6G, and MG) in 3 repetitions during a period of 8 h. The initial concentration of the organic dyes was equal to 10  $\mu$ mol/L. The volume of the solution under study equaled 100 mL, the mass of the powder of grinded shells equaled 500 mg [83], and the mass of the shells' solid material (plate—3  $\times$  3  $\times$  0.3 cm) equaled 5  $\pm$  1 g. The stirring of the solution under study was performed through the use of a magnetic mixer (200 rpm) with simultaneous horizontal shaking, at a frequency of 1 Hz. The study of dark/light sorption/desorption activity, as well as the self-decomposition of the organic dyes, was conducted by means of the Shimadzu UV-1240 spectrophotometer at wavelengths of MB—664 nm; MO—464 nm; R6G—526 nm; and MG—616 nm. The thermal control of the solutions under study was conducted by means of an Agilent G3292A Chiller. The light phase was held under radiation within the range of 320–850 nm, with a power density of 800 W/m<sup>2</sup>, using an Aqua Arc Osram lamp, Sylvania.

### 3.3. Place of Sampling Biological Items

The sampling of biological samples was carried out in Peter the Great Gulf in the Russian waters of the Sea of Japan (Figure 2). The hydrological regimen of this sea area is distinguished by a substantial seasonal and spatial variability. In summer, the Gulf's waters approach the subtropical by their properties, with the highest temperatures observed in August being up to +30 °C (the average annual August temperature equals 23.2 °C above zero). The estuarine waters are characterized by a temperature up to +23 °C and up to 31‰ of salinity, the costal surface—from +16 to +23 °C, of 31–33‰ salinity and the subsurface—from +2 to +16 °C, of 33‰ salinity [54]. The sampling of the mineral skeleton of marine invertebrates was conducted in summertime (August) from a section of a coastal discharge of 2  $\times$  2 m of size and up to 0.1 m deep. The total weight of the found fragments of the mineral skeleton in invertebrates equaled 1066 g.

### 3.4. Synthesis and Study of Photocatalyst Properties

The method for obtaining a photocatalytic coating based on Ca<sub>x</sub>Ti<sub>y</sub>O<sub>z</sub> consisted of several stages: (1) heating and holding commercial TiO<sub>2</sub> (TU80292, RUS) powder for 1 h at a temperature of 900 °C to stabilize the phase composition; (2) joint grinding in a disk mill (Herzog HSM 100) of annealed TiO<sub>2</sub> powder and *Mizuhopecten yessoensis* shells to an average particle size of 6 microns; (3) applying a layer of initial components to the surface of the *Mizuhopecten yessoensis* shell; and (4) automated point laser treatment (CO<sub>2</sub>-laser Julong-M-440-50) for 2 s per point at an installation power of 80 W.

The study of the photocatalytic properties of the resulting coating was carried out after abrasion in an agate mortar. The photocatalytic activity of the coating powder was compared with the original powder components of this coating (CaCO<sub>3</sub> and TiO<sub>2</sub>). The study of the photocatalytic activity of the resulting coating powder (100 mg) was carried out under the influence of light radiation with a power density of 800 W/m<sup>2</sup>, using an Aqua Arc Osram, Sylvania lamp (320–850 nm), in the photooxidation reaction of a model organic pollutant—methylene blue at the initial concentration of 10  $\mu$ mol/L in 100 mL of water.

#### 4. Conclusions

This paper considered the prospect of applying shells of marine invertebrates as precursor substances in the synthesis of photocatalysts and also as carriers of photocatalytic coatings. We studied the species (*Crenomytilus grayanus*, *Callista brevisiphonata*, and *Mizuhopecten yessoensis*) of marine invertebrates (phylum: *Mollusca*) from the Russian part of the Sea of Japan that are most frequently encountered in coastal discharges. We considered various properties of clam shells (physicochemical, mechanical, ecological, and exploitative) to provide a rationale of their possible use in photocatalytic applications. A high bio-indifference in the material of clam shells was shown, due to the absence in their composition of the elements hazardous to the aquatic medium and the biological objects living in it. The main component of the shell material is calcium carbonate in the modifications (calcite/aragonite), and the ratio was different for each of the studied mollusk species. The content of inorganic impurity compounds did not exceed one percent by weight. We studied the mechanical resistance of clam shells at dynamic impact (grinding) and static flexural/compression loads. A positive correlation dependency was revealed between the grindability of clam shells and the content of calcite and organic component in their composition. We studied the dependency of resistance to flexural and compressing loads from the content of micro- and macro-defects in the shell material, and we revealed the anisotropy of the durability values depending on the biological peculiarities of the shells' buildup. We considered both the physicochemical (wettability and sorption activity) properties of various surfaces of clam shells and their geometrical peculiarities. A good capability of water to wet all the studied shell surfaces was shown. The highest sorption activity was revealed by all the shells in respect to methylene blue, but the lowest was in respect of methyl orange. A pattern of improvement in the sorption activity of a whole shell relative to its powdery condition was determined. As a result of the studies, the prospects for obtaining photocatalytically active coatings on mollusk shells were shown, using the example of *Mizuhopecten yessoensis* shells. The low cost and high bio-indifference of both the carrier and the initial components of the coating, combined with confirmed photocatalytic activity, open up new opportunities for the production of water treatment materials of various compositions and purposes.

**Supplementary Materials:** The following supporting information can be downloaded at <https://www.mdpi.com/article/10.3390/catal14010016/s1>, Figure S1: Strength measurement method; Figure S2: Appearance of mollusk shells; Figure S3: EDX analysis of crushed mollusk shells.

**Author Contributions:** A.V.Z., conceptualization, methodology, investigation, validation, formal analysis, data curation, and writing—original draft; I.A.A., investigation and validation. All authors have read and agreed to the published version of the manuscript.

**Funding:** This research received no external funding.

**Data Availability Statement:** No new data were created or analyzed in this study. Data sharing is not applicable to this article.

**Acknowledgments:** The photometric studies and FTIR analysis were carried out at the «Ecological Monitoring Center» on the basis of Institute of Water and Ecology Problems FEB RAS. The SEM images, EDX, XRD, and XRF analysis were performed in the Far Eastern Center of Electron Microscopy on the basis of Institute of Tectonics and Geophysics FEB RAS.

**Conflicts of Interest:** The authors declare no conflict of interest.

#### References

1. Yi, G.C.; Xing, L.S.; Hea, J.H.; Rong, L.; Hong, Z.G.; Anna, W.; Monika, W.; Agnieszka, G.P.; Bo, L.; Qiao, X.Y.; et al. Impacts of heavy metals and medicinal crops on ecological systems, environmental pollution, cultivation, and production processes in China. *Ecotoxicol. Environ. Saf.* **2021**, *219*, 112336. [[CrossRef](#)]
2. Sami, U.K.; Ijaz, H. Impact of safe drinking water and clean fuels on health and wellbeing in Pakistan: A spatial analysis. *Groundw. Sustain. Dev.* **2021**, *15*, 100677. [[CrossRef](#)]

3. Albert, S.; Laetitia, P.; François, P.; Sergi, G.S. Photocatalytic treatment of natural waters. Reality or hype? The case of cyanotoxins remediation. *Water Res.* **2021**, *188*, 116543. [[CrossRef](#)]
4. Nafees, A.; Jerry, A.; Mohammad, Z.; Khan, S.S.; Xiao, J.Y.; Vijay, K.T.; Pablo, C.; Frederic, C. Visible light-conducting polymer nanocomposites as efficient photocatalysts for the treatment of organic pollutants in wastewater. *J. Environ. Manag.* **2021**, *295*, 113362. [[CrossRef](#)]
5. Arunpandian, M.; Selvakumar, K.; Raja, A.; Rajasekaran, P.; Ramalingan, C.; Nagarajan, E.R.; Pandikumar, A.; Arunachalam, S. Rational design of novel ternary Sm<sub>2</sub>WO<sub>6</sub>/ZnO/GO nanocomposites: An affordable photocatalyst for the mitigation of carcinogenic organic pollutants. *Colloids Surf. A Physicochem. Eng. Asp.* **2020**, *596*, 124721. [[CrossRef](#)]
6. Sumei, L.; Saisai, S.; Sha, C.; Hanbing, L.; Ziyi, L.; Yixuan, L.; Jiaying, F.; Linhua, X.; Jianrong, L. Photocatalytic degradation of hazardous organic pollutants in water by Fe-MOFs and their composites: A review. *J. Environ. Chem. Eng.* **2021**, *9*, 105967. [[CrossRef](#)]
7. Menglu, Z.; Yu, Y.; Xiaoqiang, A.; Li-an, H. A critical review of g-C<sub>3</sub>N<sub>4</sub>-based photocatalytic membrane for water purification. *Chem. Eng. J.* **2021**, *412*, 128663. [[CrossRef](#)]
8. Moses, G.P.; Elvera, L.V. WO<sub>3</sub>-based catalysts for photocatalytic and photoelectrocatalytic removal of organic pollutants from water—A review. *J. Water Process Eng.* **2021**, *40*, 101930. [[CrossRef](#)]
9. Nur Aqilah, M.R.; Wan Norharyati, W.S.; Farhana, A.; Lau, W.J.; Norhaniza, Y.; Ahmad, F.I. Review on tungsten trioxide as a photocatalysts for degradation of recalcitrant pollutants. *J. Clean. Prod.* **2021**, *309*, 127438. [[CrossRef](#)]
10. Sheikhshoae, I.; Ramezanpoura, S.; Khatamian, M. Synthesis and characterization of thallium doped Mn<sub>3</sub>O<sub>4</sub> as superior sunlight photocatalysts. *J. Mol. Liq.* **2017**, *238*, 248–253. [[CrossRef](#)]
11. Mojgan, G.; Noshin, M.; Omid, A.; Masoud, S.N. Photocatalytic degradation of antibiotic using Ni-doped thallium(I) orthotungstate nanorods: Hydrothermal synthesis and characterization. *J. Alloys Compd.* **2021**, *874*, 159856. [[CrossRef](#)]
12. Karunakaran, C.; Kalaivani, S. Enhanced visible light-photocatalysis by hydrothermally synthesized thallium-doped bismuth vanadate nanoparticles. *Mater. Sci. Semicond. Process.* **2014**, *27*, 352–361. [[CrossRef](#)]
13. Elahe, R.; Mojgan, G.; Hassan, A.A.; Maryam, K.; Mahin, B.; Masoud, S.N. Simple preparation of chitosan-coated thallium lead iodide nanostructures as a new visible-light photocatalyst in decolorization of organic contamination. *J. Mol. Liq.* **2021**, *341*, 117299. [[CrossRef](#)]
14. Renukadevi, R.; Sundaram, R.; Kaviyarasubc, K. Robust Hg<sub>0.023</sub>WO<sub>3</sub> nanoparticles: Synthesis, characterization and application as relative humidity sensing material and photocatalyst for degradation of organic dye contamination. *Nanosmatafrica* **2021**, *36*, 192–198. [[CrossRef](#)]
15. Datang, L.; Jiayin, L.; Jianting, T. Mercury oxide as an efficient photocatalyst for degradation of rhodamine B dye under visible-light irradiation. *Solid State Sci.* **2016**, *61*, 201–206. [[CrossRef](#)]
16. Zhenghua, W.; Shiyu, Z.; Suping, Z.; Haibo, H. Synthesis of core-shell Fe<sub>3</sub>O<sub>4</sub>@SiO<sub>2</sub>@MS (M = Pb, Zn, and Hg) microspheres and their application as photocatalysts. *J. Alloys Compd.* **2011**, *509*, 6893–6898. [[CrossRef](#)]
17. Yang, L.; Jian, Z.; Guangshan, Z.; Lilan, Z.; Shiyuan, D.; Enxiang, S.; Xinghui, X. Visible-light-driven photocatalytic disinfection mechanism of Pb-BiFeO<sub>3</sub>/rGO photocatalyst. *Water Res.* **2019**, *161*, 251–261. [[CrossRef](#)]
18. Huiyuan, X.; Fu, W.; Biru, L.; Xiaomin, L.; Jiayu, C.; Yang, Y.; Sen, H.; Xiaoyun, F. A novel double anion layered photocatalyst Pb<sub>4</sub>(BO<sub>3</sub>)<sub>2</sub>SO<sub>4</sub> with enhanced photocatalytic performance for antibiotic degradation. *Chem. Eng. J.* **2022**, *429*, 132344. [[CrossRef](#)]
19. Saroj, L.; Dushyant, K.P.; Anjali, S.; Shipra, B. Wastewater treatment using nanomaterial quaternary photocatalyst ZrCdPbO<sub>4</sub>—Removal of colour pollutant by an eco friendly process. *J. Indian Chem. Soc.* **2021**, *98*, 100194. [[CrossRef](#)]
20. Jiajia, L.; Ziwei, Z.; Zhuoning, L.; Huijuan, Y.; Shijun, Y.; Yuping, T.; Qizhao, W. Construction of immobilized films photocatalysts with CdS clusters decorated by metal Cd and BiOCl for photocatalytic degradation of tetracycline antibiotics. *Chin. Chem. Lett.* **2022**, *33*, 3705–3708. [[CrossRef](#)]
21. Jiajia, L.; Tianyi, L.; Ziwei, Z.; Rui, X.; Yu, L.; Ya, H.; Caiyun, Y.; Sai, Z.; Yuping, T. Preparation of heterostructured ternary Cd/CdS/BiOCl photocatalysts for enhanced visible-light photocatalytic degradation of organic pollutants in wastewater. *Inorg. Chem. Commun.* **2020**, *121*, 108236. [[CrossRef](#)]
22. Ya, N.R.; Wei, X.; Lin, X.Z.; Yue, Q.Z. Efficient tetracycline adsorption and photocatalytic degradation of rhodamine B by uranyl coordination polymer. *J. Solid State Chem.* **2017**, *251*, 105–112. [[CrossRef](#)]
23. Vinod, K.G.; Shilpi, A.; Deepak, P.; Kothiyal, N.C.; Gaurav, S. Use of pectin–thorium (IV) tungstomolybdate nanocomposite for photocatalytic degradation of methylene blue. *Carbohydr. Polym.* **2013**, *96*, 277–283. [[CrossRef](#)]
24. Saikatendu, D.R.; Krishna, C.D.; Siddhartha, S.D. Conventional to green synthesis of magnetic iron oxide nanoparticles; its application as catalyst, photocatalyst and toxicity: A short review. *Inorg. Chem. Commun.* **2021**, *134*, 109050. [[CrossRef](#)]
25. Hossein, B. Green synthesis of activated carbon doped tungsten trioxide photocatalysts using leaf of basil (*Ocimum basilicum*) for photocatalytic degradation of methylene blue under sunlight. *J. Saudi Chem. Soc.* **2022**, *26*, 101432. [[CrossRef](#)]
26. Moral-Rodríguez, A.I.; Quintana, M.; Leyva, R.R.; Ojeda-Galvánb, H.J.; Oros, R.S.; Peralta-Rodríguez, R.D.; Mendoza, M.E. Novel and green synthesis of BiVO<sub>4</sub> and GO/BiVO<sub>4</sub> photocatalysts for efficient dyes degradation under blue LED illumination. *Ceram. Int.* **2022**, *48*, 1264–1276. [[CrossRef](#)]
27. Asma, E.G.; Murilo, F.; Nicola, B.; Chérif, D.; Antonio, M.; Michele, O. Wastewater remediation with ZnO photocatalysts: Green synthesis and solar concentration as an economically and environmentally viable route to application. *J. Environ. Manag.* **2021**, *286*, 112226. [[CrossRef](#)]

28. Lusi, E.; Ruri, A.W.; Hendri, W.; Doty, D.R.; Ade, W.Y.; Rebeka, V.S. Experimental data of CaTiO<sub>3</sub> photocatalyst for degradation of organic pollutants (Brilliant green dye)—Green synthesis, characterization and kinetic study. *Data Brief* **2020**, *32*, 106099. [[CrossRef](#)]
29. Manjusha, P.; Bonamali, P. A review on CaTiO<sub>3</sub> photocatalyst: Activity enhancement methods and photocatalytic applications. *Powder Technol.* **2021**, *3889*, 274–304. [[CrossRef](#)]
30. Wenjun, W.; Fawei, L.; Beibei, Y.; Zhanjun, C.; Guanyi, C.; Meng, K.; Chao, Y.; Lian, H. The role of seashell wastes in TiO<sub>2</sub>/Seashell composites: Photocatalytic degradation of methylene blue dye under sunlight. *Environ. Res.* **2020**, *188*, 109831. [[CrossRef](#)]
31. Echabbi, F.; Hamlich, M.; Harkati, S.; Jouali, A.; Tahiri, S.; Lazar, S.; Lakhmiri, R.; Safi, M. Photocatalytic degradation of methylene blue by the use of titanium-doped Calcined Mussel Shells CMS/TiO<sub>2</sub>. *J. Environ. Chem. Eng.* **2019**, *7*, 103293. [[CrossRef](#)]
32. Sanpriet, A.; Jaspin, S.; Mahendran, R. Utilization of eggshell waste in calcium-fortified foods and other industrial applications: A review. *Trends Food Sci. Technol.* **2021**, *115*, 422–432. [[CrossRef](#)]
33. Jacobs, R.; Gordon, M.; Jerina, M. Feeding a seaweed-derived calcium source versus calcium carbonate on physiological parameters of horses. *J. Equine Vet. Sci.* **2019**, *76*, 83. [[CrossRef](#)]
34. Kena, Q.; Qingliang, Z.; Hang, Y.; Xinhui, X.; Jianju, L.; Shufei, H.; Liangliang, W.; Taicheng, A. A review of bismuth-based photocatalysts for antibiotic degradation: Insight into the photocatalytic degradation performance, pathways and relevant mechanisms. *Environ. Res.* **2021**, *199*, 111360. [[CrossRef](#)]
35. Yongjiao, W.; Yiming, H.; Tingting, L.; Jun, C.; Mengfei, L.; Leihong, Z. Photocatalytic degradation of methylene blue on CaBi<sub>6</sub>O<sub>10</sub>/Bi<sub>2</sub>O<sub>3</sub> composites under visible light. *Chem. Eng. J.* **2012**, *189–190*, 473–481. [[CrossRef](#)]
36. Shtarev, D.S.; Serpone, N. A new generation of visible-light-active photocatalysts—The alkaline earth metal bismuthates: Syntheses, compositions, structures, and properties. *J. Photochem. Photobiol. C Photochem. Rev.* **2022**, *50*, 100501. [[CrossRef](#)]
37. Zaitsev, A.V.; Kirichenko, E.A.; Kaminsky, O.I.; Makarevich, K.S. Investigation into the efficiency of photocatalytic oxidation of aqueous solutions of organic toxins in a unit with an automatically cleaning bismuth-silicate photocatalyst. *J. Water Process Eng.* **2020**, *37*, 101468. [[CrossRef](#)]
38. Zaitsev, A.V.; Makarevich, K.S.; Kaminsky, O.I.; Kirichenko, E.A.; Krutikova, V.O. Fabrication of coatings based on strontium-bismuth-silicate photocatalyst for water purification from organic pollutants. *Mater. Lett.* **2021**, *291*, 129601. [[CrossRef](#)]
39. Gomez, V.; Rome, B.; Barron, A.R.; Dunnill, C.W. Bi-Phasic photocatalytic particles prepared by sequential layer depositions for water cleaning and purification. *Nano Energy Syst.* **2016**, 5–13. [[CrossRef](#)]
40. Zaitsev, A.V.; Astapov, I.A. Prospects for creating regenerated photocatalytic materials for solar water treatment units. *Mater. Lett.* **2022**, *310*, 131509. [[CrossRef](#)]
41. Dawei, W.; Miguel, A.M.; José, A.C.M.; Fiderman, M.M.; Ivana, G.; Rodrigo, P.M.M.; Gianluca, L.P. Engineering and modeling perspectives on photocatalytic reactors for water treatment. *Water Res.* **2021**, *202*, 117421. [[CrossRef](#)]
42. David, O. Kinetics of photocatalytic, self-cleaning surfaces: A decision tree approach for determination of reaction order. *Appl. Catal. B Environ.* **2019**, *242*, 431–440. [[CrossRef](#)]
43. Tannia, V.U.; Heriberto, E.G.; Lucía, Z.F.L.; Gabriel, A.N. Synthesis and characterization of silver nanoparticles supported on Bivalve mollusk shell for catalytic degradation of commercial dyes. *J. Photochem. Photobiol. A Chem.* **2021**, *419*, 113481. [[CrossRef](#)]
44. Nguyen, T.A.H.; Ngo, H.H.; Guo, W.S.; Nguyen, T.H.H.; Soda, S.; Vu, N.D.; Bui, T.K.A.; Vo, T.D.H.; Bui, X.T.; Nguyen, T.T.; et al. White hard clam (*Meretrix lyrata*) shells media to improve phosphorus removal in lab-scale horizontal sub-surface flow constructed wetlands: Performance, removal pathways, and lifespan. *Bioresour. Technol.* **2020**, *312*, 123602. [[CrossRef](#)] [[PubMed](#)]
45. Imane, H.; Eniko, T.; Victor, G.M.; Gábor, O.; Gyula, Z.; Said, E.A.; Said, L. Pod razor (*Ensis siliqua*) shell powder as cost-effective biomineral for removal of nickel (II), copper (II) and zinc (II) from artificially contaminated industrial wastewater. *Sustain. Chem. Pharm.* **2019**, *12*, 100137. [[CrossRef](#)]
46. Mohammad, K.O.; Harini, G.; Turki, M.D.; Akshayya, C.; Asmaa, M.; Abdullah, A.A.; Walid, S.; Mostafa, A.; Hamada, A.E.; Lija, L.R.; et al. Fabrication of MnFe<sub>2</sub>O<sub>4</sub> spheres modified CeO<sub>2</sub> nano-flakes for sustainable photodegradation of MB dye and antimicrobial activity: A brief computational investigation on reactive sites and degradation pathway. *Colloids Surf. A Physicochem. Eng. Asp.* **2022**, *641*, 128566. [[CrossRef](#)]
47. Haodong, T.; Wujian, Z.; Yue, M.; Bo, X.; Zheming, N.; Shengjie, X. Investigation onto the performance and mechanism of visible light photodegradation of methyl orange catalyzed by M/CeO<sub>2</sub> (M = Pt, Ag, Au). *Mater. Res. Bull.* **2021**, *144*, 111497. [[CrossRef](#)]
48. Nurфина, Y.; Rahma, A.; Dahlang, T.; Maria, M.S.; Yuliati, H.; Cuk, I.; Munawar, K.; Dede, D. Enhanced photocatalytic degradation of rhodamine 6G (R6G) using ZnO–Ag nanoparticles synthesized by pulsed laser ablation in liquid (PLAL). *J. Alloys Compd.* **2021**, *886*, 161291. [[CrossRef](#)]
49. Qingfeng, X.; Ziyao, W.; Hui, Y.; Yajun, X.; Guangjun, N.; Wenjin, Y. Synthesis of hierarchical Cu<sub>2</sub>CdSnS<sub>4</sub> by microwave-assisted transformation from precursor for photodegradation to malachite green. *J. Alloys Compd.* **2022**, *904*, 163966. [[CrossRef](#)]
50. Aadil, B.; Deepak, S.; Bonamali, P. Highly efficient CaCO<sub>3</sub>–CaO extracted from tap water distillation for effective adsorption and photocatalytic degradation of malachite green dye. *Mater. Res. Bull.* **2019**, *116*, 1–7. [[CrossRef](#)]
51. Ibrahim, H.A.; Amr, M.N.; Tarek, A.S.E.; Ben, A.C. A novel composite silver nanoparticles loaded calcium oxide stemming from egg shell recycling: A potent photocatalytic and antibacterial activities. *J. Clean. Prod.* **2020**, *248*, 119274. [[CrossRef](#)]

52. Khadija, M.; Muhammad, A.M.; Vickie, M.; Tuan, Z.; Mohd, N.M.Z.; Zarina, A.; Farazila, B.Y. Muhammad Mazhar, Optical and photocatalytic properties of biomimetic cauliflower-like  $\text{Ca}_2\text{Mn}_3\text{O}_8\text{-CaO}$  composite thin films. *J. Solid State Chem.* **2020**, *290*, 121552. [CrossRef]
53. Karen, S.O.G.; Erick, T.A.; Miguel, Á.M.; Fiderman, M.M.; Gianluca, L.P. A Novel Prototype Offset Multi Tubular Photoreactor (OMTP) for solar photocatalytic degradation of water contaminants. *Chem. Eng. J.* **2018**, *341*, 628–638. [CrossRef]
54. Lutaenko, K.A. *Atlas of Common Bivalve Mollusks of Peter the Great Bay (Sea of Japan)*; Lutaenko, K.A., Volvenko, I.E., Adrianov, A.V., Eds.; Far Eastern Federal University: Vladivostok, Russia, 2017; p. 140. ISBN 978-5-7444-3980-4.
55. Plants and Animals of the Japan. In *East Sea: Short Field Guide*; “Phoenix” Fund, Project Aware (UK), Far Eastern State University: Vladivostok, Russia, 2007; p. 488. ISBN 978-5-7444-1966-0.
56. Frédéric, M.; Gilles, L. Molluscan shell proteins. *Comptes Rendus Palevol* **2004**, *3*, 469–492. [CrossRef]
57. Ewelina, K.W.; Jan, M.; Paweł, M. Sintering Behavior of Kaolin with Calcite. *Procedia Eng.* **2013**, *57*, 572–582. [CrossRef]
58. George, T.F. Differentiation of Aragonite from Calcite by Differential Thermal Analysis. *Science* **1949**, *110*, 402–403. [CrossRef]
59. Passe, C.N.; N’Guyen, P.; Pelmard, R.; Ouensanga, A.; Bouchon, C. Water desorption and aragonite—Calcite phase transition in scleractinian corals skeletons. *Thermochim. Acta* **1995**, *265*, 135–140. [CrossRef]
60. Yaozhuang, L.; Yuwei, F.; Zhisheng, X.; Long, Y.; Xiaojiang, X.; Zhengyang, W. Synergistic effect of clam shell bio-filler on the fire-resistance and char formation of intumescent fire-retardant coatings. *J. Mater. Res. Technol.* **2020**, *9*, 14718–14728. [CrossRef]
61. Nur, S.I.; Wai, L.L.; Daud, M.; Siti, H.A.; Hadi, N. A critical review of metal-doped  $\text{TiO}_2$  and its structure–physical properties–photocatalytic activity relationship in hydrogen production. *Int. J. Hydrogen Energy* **2020**, *45*, 28553–28565. [CrossRef]
62. Sanakousar, F.M.; Vidyasagar, C.C.; Jiménez-Pérez, V.M.; Prakash, K. Recent progress on visible-light-driven metal and non-metal doped ZnO nanostructures for photocatalytic degradation of organic pollutants. *Mater. Sci. Semicond. Process.* **2022**, *140*, 106390. [CrossRef]
63. João, V.N.; Helen, C.F.; Cristiano, P.B. Effect of seawater ionic composition modified by nanofiltration on enhanced oil recovery in Berea sandstone. *Fuel* **2017**, *203*, 222–232. [CrossRef]
64. Jorune, S.; Meaghan, M.; Alberto, J.T.; Matthew, J.C.; Frédéric, M.; Beatrice, D. The degradation of intracrystalline mollusk shell proteins: A proteomics study of *Spondylus gaederopus*. *Biochim. Biophys. Acta (BBA)—Proteins Proteom.* **2021**, *1869*, 140718. [CrossRef]
65. Charles, G. Structure of the conchiolin cases of the prisms in *mytilus edulis* linne. *J. Biophys Biochem. Cytol.* **1961**, *9*, 395–400. [CrossRef]
66. Hye, W.K.; Taekgeun, Y.; Seungkwan, H.; Seockheon, L.; Seongpil, J. Retardation of wetting for membrane distillation by adjusting major components of seawater. *Water Res.* **2020**, *175*, 115677. [CrossRef]
67. Daniella, M.; Alireza, R.Y.; Marcello, P.; Mark, T. A review of the latest insights into the mechanism of action of strontium in bone. *Bone Rep.* **2020**, *12*, 100273. [CrossRef]
68. Xinyue, Z.; Li, L.; Qianlong, Z.; Xingxing, L.; Dongxue, L. Facile synthesis of novel gully-like double-sized mesoporous structural Sr-doped  $\text{ZrO}_2\text{-TiO}_2$  composites with improved photocatalytic efficiency. *J. Solid State Chem.* **2019**, *269*, 375–385. [CrossRef]
69. Li, L.; Yang, Y.; Yirui, L.; Ping, Y.; Ting, L. Porous calcite  $\text{CaCO}_3$  microspheres: Preparation, characterization and release behavior as doxorubicin carrier. *Colloids Surf. B Biointerfaces* **2020**, *186*, 110720. [CrossRef]
70. Eyob, W.; Zelalem, C.L.; Jooheon, K. Polyisocyanate-based water-soluble polyurethane/ $\text{CaCO}_3$  composites for gunpowder storage. *Polym. Test.* **2021**, *99*, 107211. [CrossRef]
71. Oluwatoosin, B.A.; Agbaje, J.; Gabriel, D.; Dorrit, E.J. Organic biopolymers of venus clams: Collagen-related matrix in the bivalve shells with crossed-lamellar ultrastructure. *Biochem. Biophys. Rep.* **2021**, *26*, 100939. [CrossRef]
72. Emmanuel, J.M.E.; Jonyl, L.G.; Francis, M.d.R.; Eric, R.P. Sonochemical synthesis, characterization and photocatalytic properties of hydroxyapatite nano-rods derived from mussel shells. *Mater. Lett.* **2017**, *196*, 33–36. [CrossRef]
73. Luis, P.V.; Fatah, T.; Laila, M.; Bartolomé, C.H.; Dolores, E.Q.; Pedro, J.S.S. Synthesis of vaterite  $\text{CaCO}_3$  as submicron and nanosized particles using inorganic precursors and sucrose in aqueous medium. *Ceram. Int.* **2018**, *44*, 5291–5296. [CrossRef]
74. Jun, H.S.; Mark, I.J.; Darrell, A.P. Greener photocatalysts: Hydroxyapatite derived from waste mussel shells for the photocatalytic degradation of a model azo dye wastewater. *Chem. Eng. Res. Des.* **2013**, *91*, 1693–1704. [CrossRef]
75. Ju, Y.L.; Seon, H.J.; Jong, C.L. Effect of surface modification of  $\text{CaCO}_3$  nanoparticles by a silane coupling agent methyltrimethoxysilane on the stability of foam and emulsion. *J. Ind. Eng. Chem.* **2019**, *74*, 63–70. [CrossRef]
76. Simpson, L.J. Electrochemically generated  $\text{CaCO}_3$  deposits on iron studied with FTIR and Raman spectroscopy. *Electrochim. Acta* **1998**, *43*, 2543–2547. [CrossRef]
77. Silvia, M.d.P.; Marina, S. Studies on molluscan shells: Contributions from microscopic and analytical methods. *Micron.* **2009**, *40*, 669–690. [CrossRef]
78. Serkan, C. Analysis of grinding aid performance effects on dry fine milling of calcite. *Adv. Powder Technol.* **2022**, *33*, 103446. [CrossRef]
79. Clifford, Y.T.; Meng, C.C.; Shih, W.Y. Synergetic effects of temperature and magnetic field on the aragonite and calcite growth. *Chem. Eng. Sci.* **2011**, *66*, 1246–1253. [CrossRef]
80. Available online: <https://pubchem.ncbi.nlm.nih.gov> (accessed on 16 January 2023).
81. Available online: <https://www.sciencedirect.com> (accessed on 16 January 2023).

82. Suguru, N.; Shuntaro, A.; Ryo, S.; Yasuharu, K.; Shinya, Y. Key particle properties of shells for cadmium chemisorption. *Chemosphere* **2022**, *287*, 132257. [[CrossRef](#)]
83. Sunil, R.; Virendra, K.S.; Avdesh, S.P.; Mohit, N.; Kuldeep, R. Adsorption of methyl red dye from aqueous solution onto eggshell waste material: Kinetics, isotherms and thermodynamic studies. *Curr. Res. Green Sustain. Chem.* **2021**, *4*, 100180. [[CrossRef](#)]

**Disclaimer/Publisher's Note:** The statements, opinions and data contained in all publications are solely those of the individual author(s) and contributor(s) and not of MDPI and/or the editor(s). MDPI and/or the editor(s) disclaim responsibility for any injury to people or property resulting from any ideas, methods, instructions or products referred to in the content.